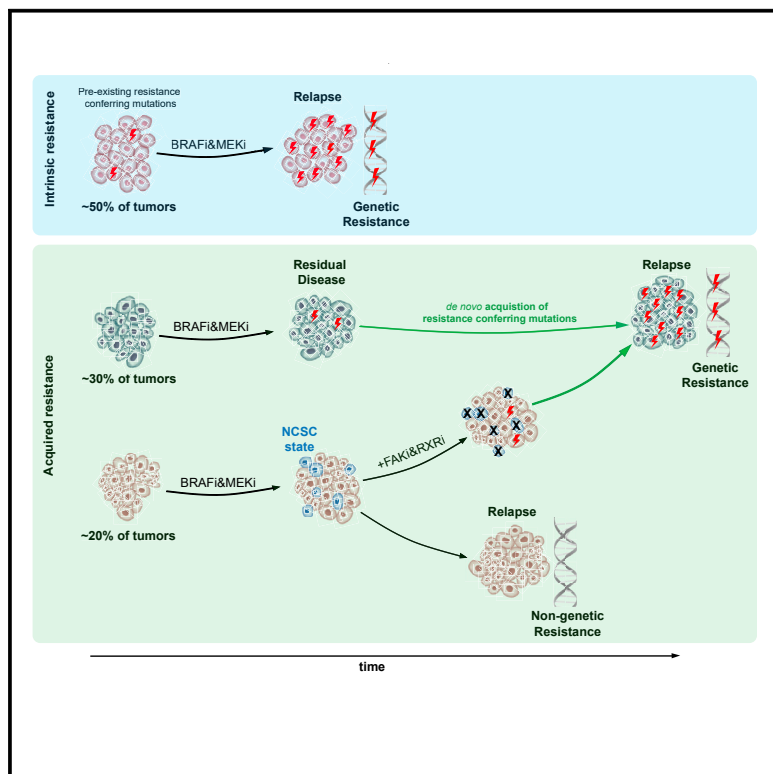


## Evolutionary predictability of genetic versus nongenetic resistance to anticancer drugs in melanoma

### Graphical abstract



### Authors

Oskar Marin-Bejar, Aljosja Rogiers,  
Michael Dewaele, ..., Amanda W. Lund,  
Florian Rambow,  
Jean-Christophe Marine

### Correspondence

florian.rambow@kuleuven.be (F.R.),  
jeanchristophe.marine@kuleuven.be  
(J.-C.M.)

### In brief

Marin-Bejar et al. identify focal adhesion kinase (FAK) as a vulnerability of melanoma drug persisters harboring a neural crest-like state. Targeting these cells, using a FAK inhibitor, prevents the development of nongenetic, but not genetic, resistance, indicating that the path to resistance is dictated by the cellular composition of minimal residual disease.

### Highlights

- Tumors recurrently select either a genetic or nongenetic drug resistance trajectory
- FAK signaling is activated in melanoma drug persisters with a neural crest-like state
- Targeting neural crest-like cells prevents nongenetic drug resistance evolution
- The cellular composition of MRD dictates the evolutionary path to resistance



## Article

# Evolutionary predictability of genetic versus nongenetic resistance to anticancer drugs in melanoma

Oskar Marin-Bejar,<sup>1,2</sup> Aljosja Rogiers,<sup>1,2</sup> Michael Dewaele,<sup>1,2</sup> Julia Femel,<sup>3</sup> Panagiotis Karras,<sup>1,2</sup> Joanna Pozniak,<sup>1,2</sup> Greet Bervoets,<sup>1,2</sup> Nina Van Raemdonck,<sup>1,2</sup> Dennis Pedri,<sup>1,2</sup> Toon Swings,<sup>4</sup> Jonas Demeulemeester,<sup>5,6</sup> Sara Vander Borght,<sup>7</sup> Stefan Lehnert,<sup>9</sup> Francesca Bosisio,<sup>8</sup> Joost J. van den Oord,<sup>8</sup> Isabelle Vanden Bempt,<sup>9</sup> Diether Lambrechts,<sup>10,11</sup> Thierry Voet,<sup>5,12</sup> Oliver Bechter,<sup>13</sup> Helen Rizos,<sup>14,15</sup> Mitchell P. Levesque,<sup>16</sup> Eleonora Leucci,<sup>17,18</sup> Amanda W. Lund,<sup>3</sup> Florian Rambow,<sup>1,2,\*</sup> and Jean-Christophe Marine<sup>1,2,19,\*</sup>

<sup>1</sup>Laboratory for Molecular Cancer Biology, Center for Cancer Biology, VIB, Leuven, Belgium

<sup>2</sup>Laboratory for Molecular Cancer Biology, Department of Oncology, KU Leuven, Leuven, Belgium

<sup>3</sup>Ronald O. Perelman Department of Dermatology and Department of Pathology, NYU Grossman School of Medicine, New York, NY, USA

<sup>4</sup>VIB Technology Watch, Technology Innovation Lab, VIB, Leuven, Belgium

<sup>5</sup>Laboratory of Reproductive Genomics, Department of Human Genetics, KU Leuven, Leuven, Belgium

<sup>6</sup>Cancer Genomic Laboratory, The Francis Crick Institute, London, UK

<sup>7</sup>Department of Pathology, UZ Leuven, Leuven, Belgium

<sup>8</sup>Laboratory of Translational Cell and Tissue Research, Department of Pathology, KU Leuven and UZ Leuven, Leuven, Belgium

<sup>9</sup>Center for Human Genetics, KU Leuven, Leuven, Belgium

<sup>10</sup>Laboratory of Translational Genetics, Center for Cancer Biology, VIB, Leuven, Belgium

<sup>11</sup>Laboratory of Translational Genetics, Center for Human Genetics, KU Leuven, Belgium

<sup>12</sup>KU Leuven Institute for Single Cell Omics, LISCO, KU Leuven, Leuven, Belgium

<sup>13</sup>Department of General Medical Oncology UZ Leuven, Belgium

<sup>14</sup>Macquarie University, Sydney, NSW, Australia

<sup>15</sup>Melanoma Institute Australia, Sydney, NSW, Australia

<sup>16</sup>Department of Dermatology, University of Zürich Hospital, University of Zürich, Zürich, Switzerland

<sup>17</sup>Laboratory for RNA Cancer Biology, Department of Oncology, LKI, KU Leuven, Leuven, Belgium

<sup>18</sup>Trace PDX Platform, Department of Oncology, LKI, KU Leuven, Leuven, Belgium

<sup>19</sup>Lead contact

\*Correspondence: [florian.rambow@kuleuven.be](mailto:florian.rambow@kuleuven.be) (F.R.), [jeanchristophe.marine@kuleuven.be](mailto:jeanchristophe.marine@kuleuven.be) (J.-C.M.)

<https://doi.org/10.1016/j.ccr.2021.05.015>

## SUMMARY

Therapy resistance arises from heterogeneous drug-tolerant persister cells or minimal residual disease (MRD) through genetic and nongenetic mechanisms. A key question is whether specific molecular features of the MRD ecosystem determine which of these two distinct trajectories will eventually prevail. We show that, in melanoma exposed to mitogen-activated protein kinase therapeutics, emergence of a transient neural crest stem cell (NCSC) population in MRD concurs with the development of nongenetic resistance. This increase relies on a glial cell line-derived neurotrophic factor-dependent signaling cascade, which activates the AKT survival pathway in a focal adhesion kinase (FAK)-dependent manner. Ablation of the NCSC population through FAK inhibition delays relapse in patient-derived tumor xenografts. Strikingly, all tumors that ultimately escape this treatment exhibit resistance-conferring genetic alterations and increased sensitivity to extracellular signal-regulated kinase inhibition. These findings identify an approach that abrogates the nongenetic resistance trajectory in melanoma and demonstrate that the cellular composition of MRD deterministically imposes distinct drug resistance evolutionary paths.

## INTRODUCTION

The inability to fully eradicate metastasis, the major source of cancer-related deaths, remains one of the most important clinical challenges. Despite promising advances in cancer care, the vast majority of patients who initially respond to treatment, later develop resistance. This is because most available thera-

peutic modalities, even if combined, almost invariably leave a reservoir of residual cancer cells behind, traditionally called minimal residual disease (MRD), from which relapse inevitably emerges.

The most commonly accepted explanation for the inexorable evolution of resistance invokes genetic alterations (Holohan et al., 2013). Recent findings, however, indicate that drug-tolerant



persister (DTP) phenotype(s) (defined as the ability to survive the drug treatment) can be transiently acquired through non-mutational mechanisms (Menon et al., 2015; Rambow et al., 2018; Roesch et al., 2013; Sharma et al., 2010; Su et al., 2017; Trumpp and Wiestler, 2008). Studying the response of BRAF-mutant melanoma to mitogen-activated protein kinase (MAPK)-targeted therapy, we reported the co-emergence of varying combinations of distinct DTP transcriptional states (Rambow et al., 2018). Four distinct melanoma DTP cell states were identified: the starved melanoma cell (SMC) state sharing transcriptomic features of nutrient-deprived cells (Kondo et al., 2017), a neural crest stem-like cell (NCSC) state, an invasive or mesenchymal-like state that was recently renamed an undifferentiated state (Rambow et al., 2019; Tsoi et al., 2018) and a hyperdifferentiated state. Interestingly, the NCSC transcriptional program is largely driven by the nuclear receptor RXR and, consistently, an RXR antagonist (HX531) mitigates, but does not prevent, accumulation of NCSCs in MRD and delays the development of resistance (Rambow et al., 2018). These data illustrate the potential of MRD-directed therapies (Luskin et al., 2018) and indicate that the pool of NCSCs can serve as the cellular origin of drug resistance. However, since no RXR antagonist has been approved by the FDA to date, translating this work into a new treatment requires the identification of more efficient and clinically compatible approaches to target these cells.

Drug resistance (which, as opposed to tolerance, designates the ability to proliferate despite therapy exposure) may also develop in the absence of detectable genetic alterations (Bell et al., 2019; Fong et al., 2015; Hugo et al., 2015; Kim et al., 2018; Knoechel et al., 2014; Shaffer et al., 2017; Shlush et al., 2017; Woolston et al., 2019). Genomic analyses failed to identify a genetic cause for the development of stable MAPK-resistant melanoma cell cultures and lesions that regrew in drug-exposed PDXs and human patients (Bell et al., 2019; Hugo et al., 2015; Rizos et al., 2014; Shaffer et al., 2017; Shi et al., 2014). Given that melanoma is the tumor type with the highest mutation load, these observations raise the possibility that nongenetic resistance may actually be common. An improved understanding of the mechanisms underlying nongenetic drug resistance may therefore yield impactful therapeutic strategies across tumor types (Arozarena and Wellbrock, 2019; Flavahan et al., 2017; Marine et al., 2020; Pogrebniak and Curtis, 2018).

## RESULTS

### Nongenetic resistance to MAPK inhibition and induction of the NCSC state are recurrent events in human melanoma

To assess the extent to which nongenetic mechanisms contribute to resistance to targeted therapy in melanoma we performed a multicentric meta-analysis of whole-exome sequencing (WES) datasets from clinical samples ( $n = 64$ ) that progressed on combinations of BRAF and MEK inhibitors (Figure 1A; Table S1). About 20% of the samples exposed to this treatment did not exhibit any evidence of single-nucleotide alterations previously validated as drivers of resistance to MAPK therapeutics (Long et al., 2014; Rizos et al., 2014; Shi et al., 2014; Spagnolo et al., 2014) nor amplification of the *BRAF* gene, one of the most common resistance-conferring genetic al-

terations (Xue et al., 2017). Although these observations do not formally exclude the possibility that resistance may be driven in some of these samples by, for instance, non-annotated SNPs, they raised the possibility that tumor recurrence may occur in the absence of specific genetic alterations.

We previously identified a DTP cell population as a putative driver of melanoma recurrence (Rambow et al., 2018), which exhibits a gene expression signature that shows significant enrichment with NCSC signatures, such as the Lee\_Neural\_Crest\_Stem\_Cell\_UP signature ( $n = 147$  genes, systemic name = M2506) (Figure S1A) (Lee et al., 2007). Interestingly, analysis of RNA sequencing (RNA-seq) datasets from cohorts of untreated and matched drug-exposed clinical samples ( $n = 49$ ) revealed that the DTP NCSC gene expression signature was enriched in about 28% of the samples exposed to RAF/MEK inhibitors when compared with matched treatment-naïve counterparts (Figures 1B, 1C, and S1B–S1E; Table S1). Consistently, an increase in cells positive for both NCSC markers, AQP1 and NGFR, could be detected in two out of ten drug-exposed clinical samples analyzed. Importantly, these cells were only detected in samples that exhibited a partial response, but absent from samples that did not respond, to the RAF/MEK inhibitor combinations (Figure 1C). Together, these data indicated that the NCSC population emerges in about 20% of ON treatment (O/T) clinical samples and raised the possibility that these cells may function as the cellular origin of nongenetic tumor recurrence. Unfortunately, the number of clinical samples for which an in-depth longitudinal analysis was performed was too low to firmly establish this. To test this possibility, we therefore chose to use patient-derived xenografts (PDXs) as relevant *in vivo* preclinical models. These models permit facile sampling of MRD lesions, as well as to perform intervention and mechanistic studies.

### Melanoma PDX lesions recurrently select either a genetic or nongenetic drug resistance trajectory

We probed the diversity of escape mechanisms to a combination of BRAF (i.e., dabrafenib) and MEK (i.e., trametinib) inhibitors in cohorts of BRAF-mutant PDXs, all established from treatment-naïve patients. The treatment inhibited tumor growth to various degrees in almost all PDX models tested ( $n = 10$ ), but eventually all mice progressed ON treatment (Figures 2A–2C). Strikingly, although the response rates and median survivals varied considerably between models they were, by and large, comparable between mice of the same model. Two distinct behaviors were observed: whereas drug responses were relatively modest and limited in time for MEL005, MEL007, MEL017, MEL029, and MEL037 (group 1), those of MEL003, MEL006, MEL008, and MEL015 were more marked and tumor regrowth only observed after extended periods of drug tolerance (group 2). These distinct response curves are in keeping with the various clinical behaviors observed upon long-term follow-up of BRAF-mutant melanoma patients (Robert et al., 2019). Whereas group 1 reflected what is commonly referred to as intrinsic resistance, group 2 mimicked acquired resistance (group 2). Note that MEL047 was established from a *BRAF*<sup>K601E</sup>-mutant lesion. The relatively weaker anti-tumor response in this model comes from the fact that it is largely driven by MEK inhibition, as the affinity of dabrafenib for this particular *BRAF* mutation is drastically reduced (Rogiers et al., 2019).

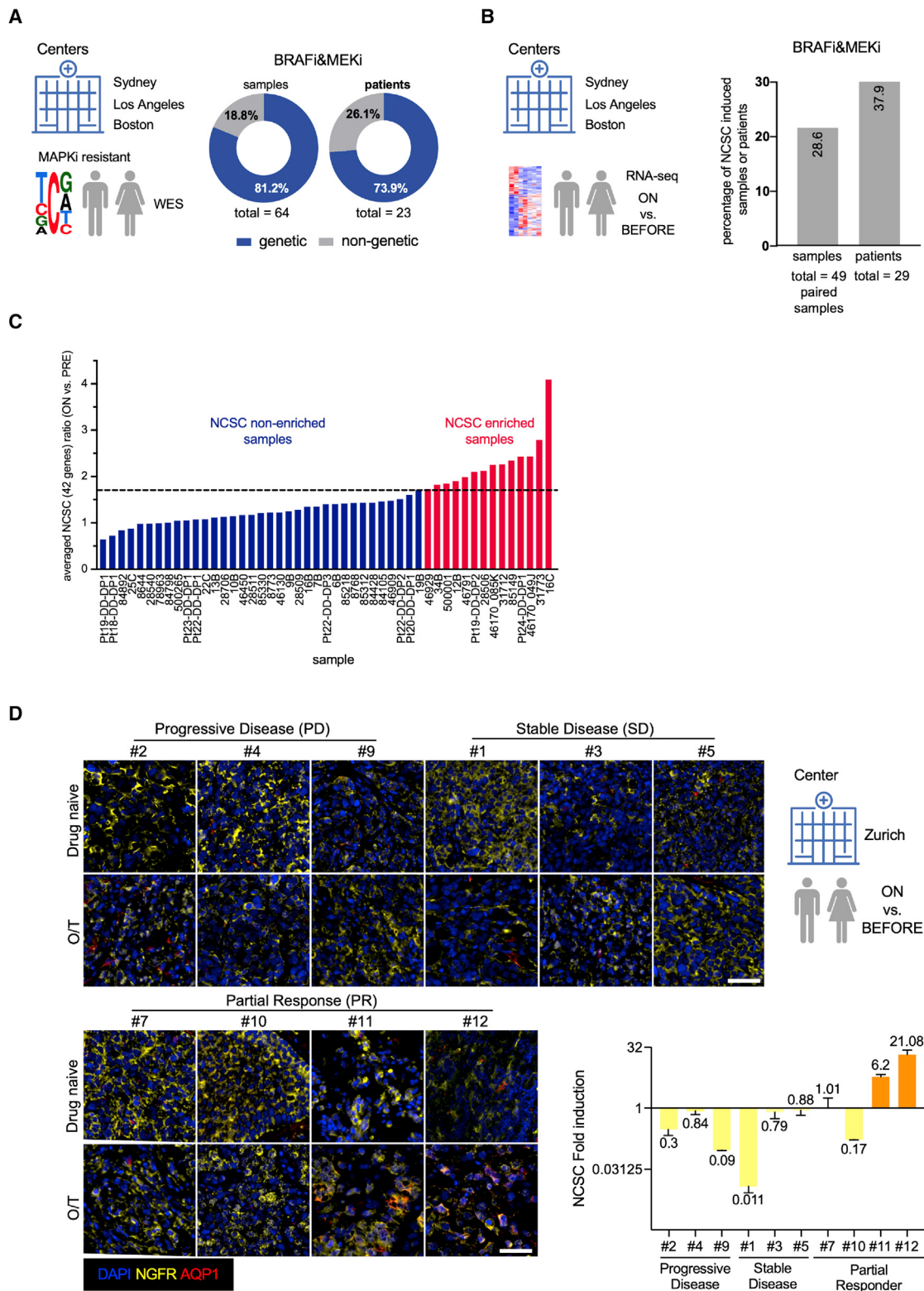


**Figure 1. Nongenetic resistance to MAPK inhibition and the induction of the NCSC state are frequent events in human melanoma**  
(A) MAPKi-resistant human melanoma samples were analyzed by whole-exome sequencing (WES) for absence (nongenetic) or presence of genetic events (Hugo et al., 2015; Kwong et al., 2015; Long et al., 2014). The analysis included samples from the Melanoma Institute Australia (Sydney, Australia), Massachusetts

To dissect the mechanisms underlying therapy resistance, we subjected drug-naïve (T0) and resistant (TRes) lesions from each of the PDX models from groups 1 and 2 to bulk targeted DNA sequencing analysis. We interrogated 26 or 96 loci (TruSight Tumor 26 kit, Illumina, or an in-house developed 96 cancer gene panel) for the presence of SNVs that are clinically prevalent and/or validated as drivers of resistance to MAPK therapeutics (Long et al., 2014; Rizos et al., 2014; Shi et al., 2014; Spagnolo et al., 2014), and measured *BRAF* copy number. The targeted DNA sequencing as well as whole-exome and SNP array data were submitted to the European Genome Archive (EGA: EGAS00001005314). We detected resistance-conferring genetic event(s) at T0 from all PDXs from group 1 (Figure 2D), indicating that intrinsic resistance in these models is driven by the pre-existence of drug-resistant subclones. In contrast, drug-resistance-conferring alterations were absent from all T0 lesions collected from models belonging to group 2. Notably, all resistant tumors collected from the MEL015 cohort (Bell et al., 2019) exhibited at least one drug-resistance-conferring alteration (Figure 2D). Single-cell targeted DNA sequencing further confirmed the presence of *NRAS* resistance-conferring mutation in one of the MEL015 TRes samples, but not in the form of rare pre-existing subclone at T0 (Figure S2A). Evidence of *BRAF* amplification was detected in MEL008 and all, but one, MEL003-resistant lesions analyzed (Figure 2D). These analyses therefore indicated that these genetic alterations are likely to be acquired *de novo* and were major drivers of the tolerance to resistance switch in these models. Strikingly, the same customized assay did not identify any resistance-conferring event in T0 or in any of the MEL006 (0/10) and MEL047 (0/5) lesions that re-emerged under dabrafenib-trametinib (DT) (Figure 2D), raising the possibility that drug resistance may be systematically driven by nongenetic mechanisms in these PDX models. To further rule out the possibility that MEL006 tumors acquire SNVs that are not represented in our targeted screening assay, we performed WES in matching parental (T0, n = 2) and drug-resistant (TRes, n = 5) lesions. This analysis did not reveal the presence of any candidate drug-resistance-conferring mutations in any of the samples analyzed (Figure 1C and data not shown). The vast majority of short variants observed are parental (total 74 indels and 3,860 single- and double-nucleotide variants) and display the mutational footprint of past UV exposure (COSMIC single-base substitution signature SBS7a/b; Figure 2E). In comparison, the TRes lesion accumulated few additional variants (11 indels and 73 single- and double-nucleotide variants), most of which can be attributed to the activity of the endogenous clock-like mutational processes SBS1 and SBS5 (Figure 2E). Likewise, the allele-specific copy-number profiles of T0 and

TRes, derived from matching SNP array data, are highly similar, with T0 having one fewer copy of chromosome 7 and an additional copy of chromosome 17 (Figure S2B). While causal drivers of resistance may fail to be identified using the above approaches, selection and expansion of a DT-resistant clone is expected to increase the variant allele frequencies of all passenger mutations present in that clone (Nik-Zainal et al., 2012; Williams et al., 2018). However, the TRes purity- and copy-number-normalized allele frequency distribution (cancer cell fractions) highlights the absence of a single selected, genetically distinct clonal population (Figure S2D). These data demonstrated that resistance to DT in the MEL006, but not MEL015, PDX models systematically resulted from the expansion of a drug-tolerant subpopulation of cells that acquire the ability to grow ON treatment through nongenetic reprogramming. Consistently, resistant lesions from MEL006, but not MEL015, responded to a DT re-challenge following their transplantation and expansion in the absence of therapy (drug holiday; Figure S2E).

Together, these analyses confirmed that PDXs are suitable to study the mechanisms underlying drug resistance as the diversity of responses seen in patients is recapitulated in these pre-clinical models (Robert et al., 2019). Unexpectedly, the type of response was very consistent between mice bearing tumors derived from the same patient. Resistance was invariably established through a non-mutational adaptive process in MEL006 and acquisition of *de novo* genetic alterations in MEL015. This observation raises the intriguing possibility that whether resistance occurs through genetic or nongenetic mechanisms may be patient dependent, deterministic, and therefore potentially predictable.

### Focal adhesion kinase signaling is selectively activated in NCSCs

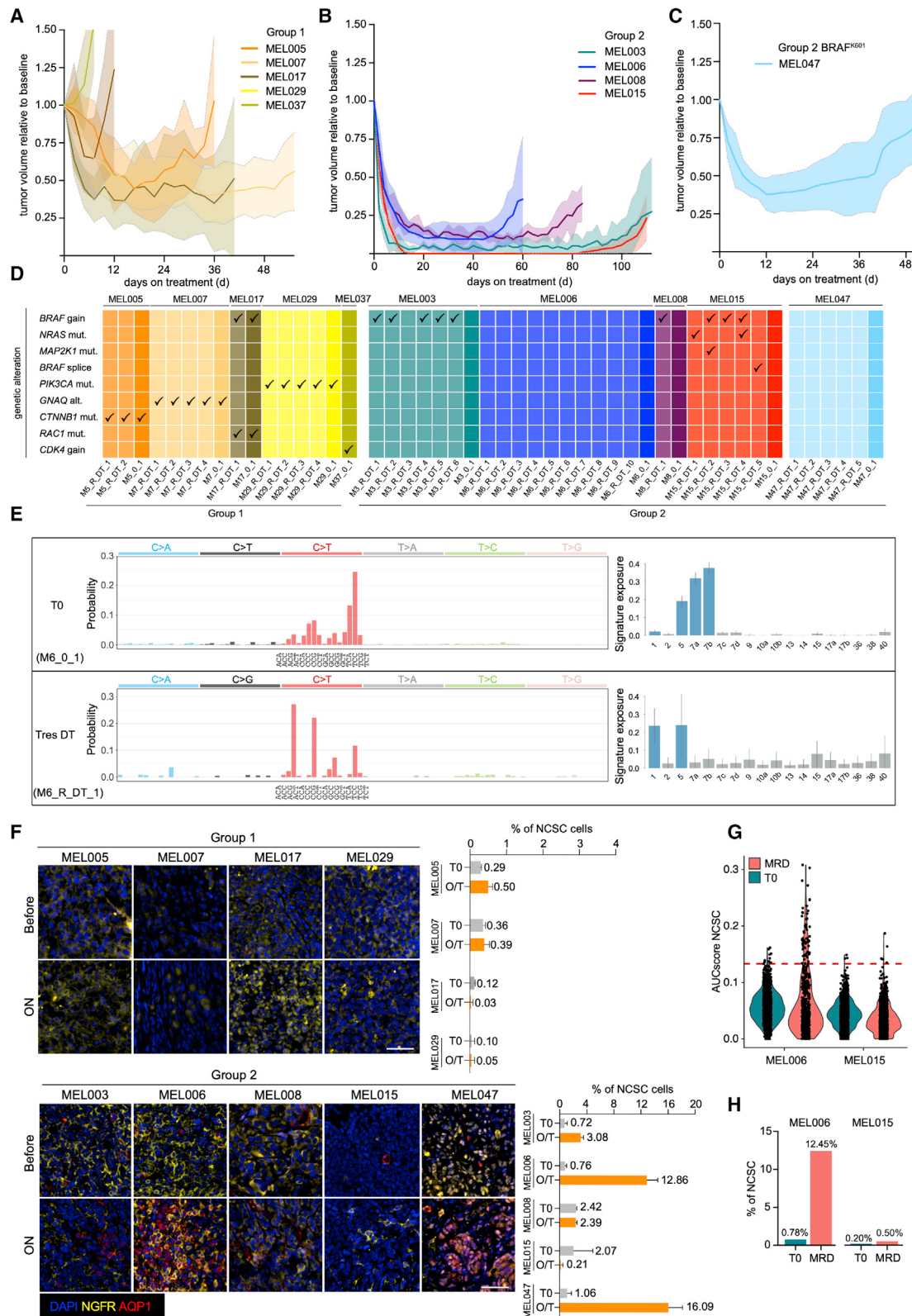
The clinical data reported in Figure 1 pinpointed the NCSC population as the putative cellular origin of nongenetic relapse. Consistently, the NCSC population was either poorly or not detected in lesions from group 1 PDXs, which exhibited intrinsic resistance to MAPK therapy (Figures 2F and S2F). Immunohistochemistry (IHC) analysis also failed to detect enrichment of NCSCs' markers in MRD from all three models in which resistance consistently occurs through *de novo* acquisition of genetic alterations (MEL015, MEL003, and MEL008). Note that we only score cells that were positive for both NCSC markers, AQP1 and NGFR. NGFR-positive/AQP1-negative cells could be detected in various lesions both before or ON treatment, but their presence did not correlate with response. Strikingly, DT exposure led to a robust increase in the NCSC population in lesions from MEL006 and MEL047 (Figures 2F and S2C). This increase

General Hospital (Boston, USA), and UCLA Dermatology (Los Angeles, USA). The percentages of samples or patients were determined for genetic and nongenetic resistance.

(B) Gene expression data (bulk RNA sequencing) of melanoma from drug-naïve samples/patients and after exposure to MAPK inhibitors were assessed for the induction of the NCSC transcriptional program. The analysis included samples from the Melanoma Institute Australia (Sydney, Australia), UCLA Dermatology (Los Angeles, USA), and Massachusetts General Hospital (Boston, USA) (Hugo et al., 2015; Kwong et al., 2015; Long et al., 2014; Rizos et al., 2014).

(C) Averaged ratios of all 42 NCSC genes were plotted by sample pair (treated versus baseline) and ordered increasingly. Samples with an average ratio >1.73 were considered to be NCSC enriched.

(D) Immunostainings show emergence of AQP1+/NGFR+ double-positive NCSCs upon MAPK inhibition (O/T = ON treatment) in clinical samples from responders, but not from patients that progressed or exhibited stable disease ON treatment. Representative images are shown (the error bars represent standard deviations, n = 5 fields per tumor sample). The analysis included samples from University of Zürich Hospital (Zürich, Switzerland).



(legend on next page)

in NCSCs in MEL006, but not MEL015, MRD lesions was further confirmed by single-cell RNA sequencing (scRNA-seq) experiments (Figures 2G and 2H).

We therefore reasoned that the cellular composition of MRD may be a key deterministic factor in the decision to engage a genetic versus nongenetic mechanism of resistance, and hypothesized that the presence of the NCSCs, a cell population with increased stem cell properties (Figure S2G), may favor nongenetic resistance. To test this possibility, we needed to develop an efficient pharmacological approach that fully eradicates these cells from MRD. We therefore searched for NCSC-specific molecular vulnerabilities. Gene set enrichment analysis (GSEA) of scRNA-seq data from individual drug-tolerant cells present in MRD of MEL006 PDX (Rambow et al., 2018) indicated that focal adhesion kinase (FAK) signaling is the most significantly enriched gene expression signature in the NCSC population (Figure 3A) using the KEGG database as GSEA reference (Subramanian et al., 2005). This activation appeared specific as it was not detected in the other two DTP states present in MEL006 MRD (i.e., SMCs and hyperdifferentiated cells; Figure S3A). IHC of MEL006 MRD confirmed selective expression of the activated/phosphorylated form of FAK (pFAK) in geographically localized clusters of NCSCs, which are defined here as double positive for the NCSC markers NGFR and AQP1 (Figure 3B-C). Cells positive for GFRA2, another NCSC discriminative marker (Rambow et al., 2018), were then isolated by, fluorescence-activated cell sorting, from an *in vitro* culture of MEL006 cells exposed to DT (Figure 3D). High levels of pFAK were detected in GFRA2-positive cells by western blotting. Note that the FAK signaling cascade is activated in many cancers as it confers a cellular proliferative and/or survival advantage by inducing, among others, activation of the AKT pathway in cancer stem cells (Schober and Fuchs, 2011; Tai et al., 2015). Accordingly, levels of AKT phosphorylation were elevated in GFRA2-positive cells (Figure 3D).

Elevated integrin  $\beta$ 1/FAK/Src signaling in melanoma cells was shown to result from paradoxical activation of melanoma-associated fibroblasts by the BRAF inhibitor and the promotion of matrix production and remodeling (Hirata et al., 2015). However, FAK activation in NCSCs following MAPK inhibition did not appear to be strictly dependent on extrinsic factors. DT exposure indeed

induced phosphorylation of FAK (and AKT) in *BRAF<sup>V600E</sup>*-mutant melanoma cultures that exhibit a stable NCSC gene expression profile (i.e., MM383 cell line; Figures 3E, S3B, and S3C). As expected, extracellular signal-regulated kinase (ERK) activation was strongly inhibited by this treatment (Figure 3E). Notably, drug exposure triggered a further increase in the expression of GFRA2 and of another NCSC marker, *GDNF* (Figure 3E). This observation indicated that MAPK inhibition triggers FAK signaling in NCSC melanoma cells in a cell-autonomous manner.

GFRA2 is a transmembrane receptor of the glial cell line-derived neurotrophic factor (GDNF) family ligands (GFLs) and an essential transducer of GFL-mediated activation of signaling pathways that promote survival of several neuronal populations in the central and peripheral nervous system (Airaksinen and Saarma, 2002; Paratcha and Ledda, 2008). The survival FAK and phosphatidylinositol 3-kinase-AKT pathways are among the pathways activated by GFRA2-dependent GFL-mediated signaling (Airaksinen and Saarma, 2002; Paratcha and Ledda, 2008). As expected, the NCSC marker *GDNF*, one of the GFL ligands, is expressed in GFRA2<sup>high</sup> cells (Figure S3B), raising the possibility that FAK activation in NCSCs may be engaged by a GFRA-dependent autocrine loop. Consistently, increasing levels of *GDNF* were measured in the culture medium of MM383 exposed to DT (Figure S3D). Strikingly, addition of recombinant GDNF alone to the culture medium of MM383 was sufficient to trigger FAK activation and its downstream targets SRC and AKT, even in the absence of DT (Figure 3F). Treatment with a pharmacological inhibitor of FAK (PF562271, referred to hereafter as PF) confirmed the epistatic relationship with FAK and downstream targets SRC and AKT (Figure 3F). Moreover, silencing of *GFRA2*, *GDNF*, and *FAK* by small interfering RNA compromised DT-induced AKT activation in these cells (Figures 3G and S3E). In contrast, silencing of another GDNF receptor, *GFRA1*, the expression of which is not induced by DT, did not compromise DT-induced AKT activation. These findings indicated that NCSCs exposed to MAPK inhibitors are capable of engaging the AKT survival pathway in an autocrine fashion through a GDNF-GFRA2-FAK/SRC signaling cascade.

Interestingly, exposure of an *in vitro* culture of MEL006 PDX to conditioned medium from two distinct NCSC lines, the *BRAF*-mutant MM383 and *NRAS*-mutant WM852, led to an

## Figure 2. Establishment of *in vivo* models of nongenetic drug resistance

- (A) Relative tumor volume in function of time from group 1 *BRAF*-mutant PDXs exposed to BRAF/MEK inhibitors (DT). Group 1; MEL005 (n = 6 mice, orange), MEL007 (n = 6 mice, light orange), MEL017 (n = 6, brown), MEL029 (n = 6, yellow), MEL037 (n = 6, olive green) exposed to DT until resistance. Data are represented by mean (thick line)  $\pm$  SEM (filled area).
- (B) Relative tumor volume in function of time from group 2 *BRAF<sup>V600E</sup>*-mutant PDXs exposed to BRAF/MEK inhibitors (DT). MEL003 (n = 6 mice), MEL006 (n = 18 mice, blue), MEL008 (n = 6, burgundy), MEL015 (n = 6 mice, red) exposed to DT until resistance. Data are represented by mean (thick line)  $\pm$  SEM (filled area).
- (C) Relative tumor volume in function of time from group 2 *BRAF<sup>K601E</sup>*-mutant PDXs exposed to BRAF/MEK inhibitors (DT). MEL047 (n = 6 mice) were exposed to DT until resistance. Data are represented by mean (thick line)  $\pm$  SEM (filled area).
- (D) Interrogation of known genetic driver events of BRAFi&MEKi resistance, including BRAF-mutant splicing variants, in drug-naive lesions (o) and resistant (DT) lesions from *BRAF*-mutant PDXs using both targeted DNA sequencing and RT-PCR approaches.
- (E) Mutation spectrum of the parental (T0) MEL006 PDX lesion (upper left panel). Mutation types are color-coded and indicated on top. Trinucleotide contexts are indicated for the C > T mutations and their order is maintained across the other types. COSMIC v.3 single-base substitution signature exposures for T0 (upper right panel). Sufficiently non-zero signatures are colored blue. Mutation spectrum of MEL006 PDX lesion (TRes) compared with T0 (lower left panel) and COSMIC v.3 single-base substitution signature exposures for TRes (lower right panel).
- (F and G) (F) Immunostainings show the emergence of AQP1/NGFR-double-positive NCSCs upon MAPK inhibition (O/T = ON treatment) in MRD lesions from the MEL006 and MEL047 PDX models. Representative images are shown (the error bars represent standard deviations, n = 5 fields per tumor sample). (G) Single-cell RNA sequencing of about 20k melanoma cells before treatment (T0) and at MRD showing emergence of the NCSC state (based on the AUCell score) in the MEL006, but not MEL015, PDX model.
- (H) Quantification of single cells from (G) harboring the NCSC state at T0 versus MRD.

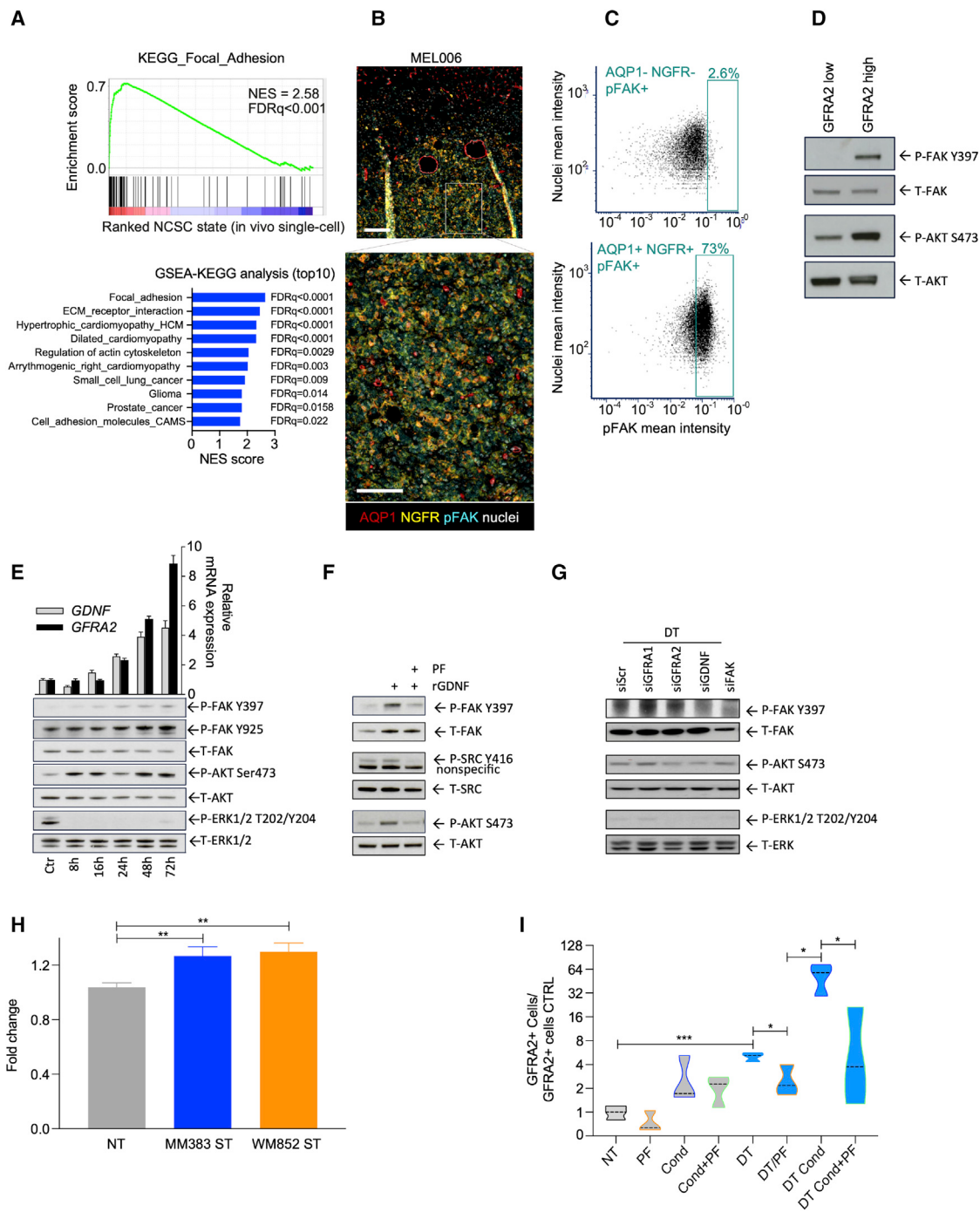


**Figure 3. FAK signaling is selectively activated in NCSCs**

- (A) Gene set enrichment analysis, using the KEGG as a reference database, identifies the focal adhesion expression program as the most enriched in the NCSC state. NES, normalized enrichment score; FDR, false discovery rate.
- (B) Multiplex immunostaining for AQP1 (red), NGFR (yellow), pFAK (cyan), and nuclei (white) at MRD after DT treatment. Representative high (top panel). Scale bars, 100  $\mu$ m and 500  $\mu$ m (low [bottom panel] magnification images are shown).
- (C) Representative image cytometry plots of pFAK intensity in AQP1<sup>-</sup>NGFR<sup>-</sup> and AQP1<sup>+</sup>NGFR<sup>+</sup> cells in MEL006 MRD lesions.
- (D) Western blot analysis of total and phosphorylated levels of FAK and AKT in GFRA2<sup>LOW</sup> and GFRA2<sup>HIGH</sup> cell populations isolated from an *in vitro* MEL006 culture exposed to DT for 72 h.
- (E) Time series monitoring induction of FAK phosphorylation (and ERK inactivation) after DT (100 nM/20 nM) exposure for 72 h in the NCSC-like cell line MM383. Control samples were treated with DMSO. Top graph shows qRT-PCR analysis of GDNF and GFRA2 expression at the indicated time points. Mean (n = 3); bars,

(legend continued on next page)

upregulation of the number of cells positive for the NCSC markers GFRA2 and NGFR (Figures 3H and S3F). We had previously shown that undifferentiated melanoma cells, such as MM099, are capable of switching ON the NCSC phenotype upon concurrent BRAF and/or MEK inhibition and that therapy-induced emergence of NCSCs can be attenuated by using the RXR signaling antagonist HX531 (HX) (Rambow et al., 2018). Consistently, activation of FAK (and SRC) and its downstream target AKT was observed in MM099 exposed to DT and this was attenuated by HX and a pharmacological inhibitor of FAK (PF; Figure S3G). Importantly, an increase in GFRA2-positive cells was also observed after exposure of these cells to MM383 conditioned medium (Figure 3I). This effect was exacerbated when the conditioned medium was collected after exposure of MM383 cells to DT, but not when cells were exposed to a DT/PF combination. These data indicated that the NCSC transcriptional program can be propagated in a paracrine fashion.

Importantly, a significant correlation was observed between the activities of both FAK and RXR signaling pathways and the NCSC gene expression signatures in large clinical cohorts, highlighting the clinical relevance of the above findings (Figure S3H).

### Targeting NCSCs through FAK inhibition delays the onset of therapy resistance

These data indicated that pharmacological inhibition of FAK signaling may offer a clinically compatible therapeutic avenue to block emergence of NCSCs in MRD. Small-molecule FAK inhibitors have indeed been developed and showed anti-tumor efficacy in several preclinical studies, including melanoma (Fallahi-Sichani et al., 2017; Hirata et al., 2015), and limited adverse effect in patients (Mousson et al., 2018). Accordingly, several FAK inhibitors are currently being evaluated in clinical trials across a range of malignancies (Mousson et al., 2018). Interestingly, exposure to two different FAK inhibitors, PF and defactinib, diminished the drug-dependent emergence of GFRA2-high cells in the MEL006 *in vitro* culture system (Figures 4A and S4A). Importantly, this effect could also be observed in various melanoma cultures, including a MEL047 culture (Figure S4C). For instance, exposure to DT/PF led to a significant decrease in growth and concomitant increase in apoptotic cell death in GFRA2-high, but not GFRA2-low, cells isolated from an MM383 NCSC culture (Figures 4B and 4C). Exposure to zVAD, a pan-caspase inhibitor, significantly reversed this effect (Figure 4C). Thus, inhibition of FAK signaling compromises the viability of NCSCs exposed to MAPK inhibitors *in vitro*.

Given the important contribution of NCSCs in the development of therapy resistance, combining PF with MAPK therapeutics may significantly limit the risk of relapse. To test the therapeutic potential of this regimen, we first assessed the impact of PF on the cellular composition of MEL006 MRD. We performed IHC analyses on MRD materials from mice treated with DT and DT/PF. While, as expected, an increase in NCSC markers was observed in MRD isolated from mice treated with DT, this was dramatically attenuated upon exposure to the triple combination (DT/PF; Figures 4D and 4E). Likewise, and consistent with our previous study (Rambow et al., 2018), exposure to HX also decreased the therapy-induced emergence of NCSCs at MRD. These decreases were accompanied by a relative increase in cells positive for CD36 and MLANA, which mark the SMC and hyperdifferentiated drug-tolerant cell populations, respectively. Strikingly, the number of NCSCs present in MRD from mice treated with the quadruple combination DT/PF/HX dropped even further, so much so that none could be detected in most lesions analyzed. Histological analysis (H&E staining) showed a progressive increase in highly pigmented (hyperdifferentiated) melanoma cells from MRD lesions exposed to DT, DT/PF, and DT/PF/HX and a concomitant decrease in tissue integrity due to necrosis and edema (Figure S4B). An scRNA-seq experiment confirmed the absence of cells harboring the NCSC gene expression signature in MRD lesions from mice treated with DT/PF/HX (Figures 4F and S4D).

Importantly, PF administration increased significantly the response rates to the DT/HX combination (Figures S4E and S4F). Moreover, combining PF with DT or DT/HX produced a significantly longer median progression-free survival (PFS) period compared with the DT or DT/HX treatments alone and delayed the development of resistance (Figure 4G; median PFS for DT = 52 days, DT/HX = 94 days, DT/PF = 104 days, and DT/PF/HX = 180 days). These treatments did not cause any relevant adverse reaction or weight loss (Figure S4G). It is noteworthy that, although the DT/PF combination was slightly superior than DT in delaying tumor recurrence in the MEL015 PDX model, the effect was far less pronounced than in the MEL006 cohorts (Figure S4H). These data identified a clinically compatible methodology that efficiently prevents the accumulation of NCSCs in MRD.

### NCSCs are key drivers of the nongenetic resistance trajectory

The ability to efficiently abrogate the emergence of NCSCs in an *in vivo* clinically relevant setting gave us the opportunity to

SD. The bottom panel shows a representative western blot analysis of the levels of pan-FAK, phosphorylated FAK at the two phosphorylation sites (position Y397 and Y925); pan-AKT, phosphorylated AKT; pan-ERK1/2 and phosphorylated-ERK1/2.

(F) Western blot analysis of overnight serum-starved MM383 cells stimulated with 100 ng/mL rGDNF for 1 h in the presence (2 h pre-treatment before stimulation) or absence of 1 μM FAKi PF562271 (PF). Levels of pan- and phosphorylated FAK, AKT, and SRC are shown.

(G) Small interfering RNA (80 nM) knockdown of *GFRA1*, *GFRA2*, *GDNF*, and *FAK* in MM383 upon inhibition of MAPK using DT (100 nM/20 mM) for 72 h. Western blot analysis shows the status of FAK, AKT, and ERK signaling.

(H) Quantification of GFRA2/NGFR-double-positive NCSCs by flow cytometry analysis in non-treated MEL006 cells (NT) and MEL006 cultured in medium supplemented with concentrated supernatant from cultures of MM383 and WM852 cells, containing a high proportion of NCSCs. Error bars represent SD of three biological replicates; \*\*p < 0.01, Mann-Whitney test.

(I) Quantification of GFRA2+ cells by flow cytometry in short-term cultures from the undifferentiated melanoma cell line MM099 (gray) before (NT) and after 10 days of treatment with 500 nM FAKi PF562271 (PF), conditioned medium from MM383 cells (Cond) and conditioned medium plus FAKi (Cond + PF). The experiments were repeated in the presence of BRAF/MEK inhibition, dabrafenib (20 nM) and trametinib (4 nM) (DT) (blue). The violin plots represent three biological replicates; \*p < 0.05, \*\*p < 0.01, \*\*\*p < 0.001, Mann-Whitney test.

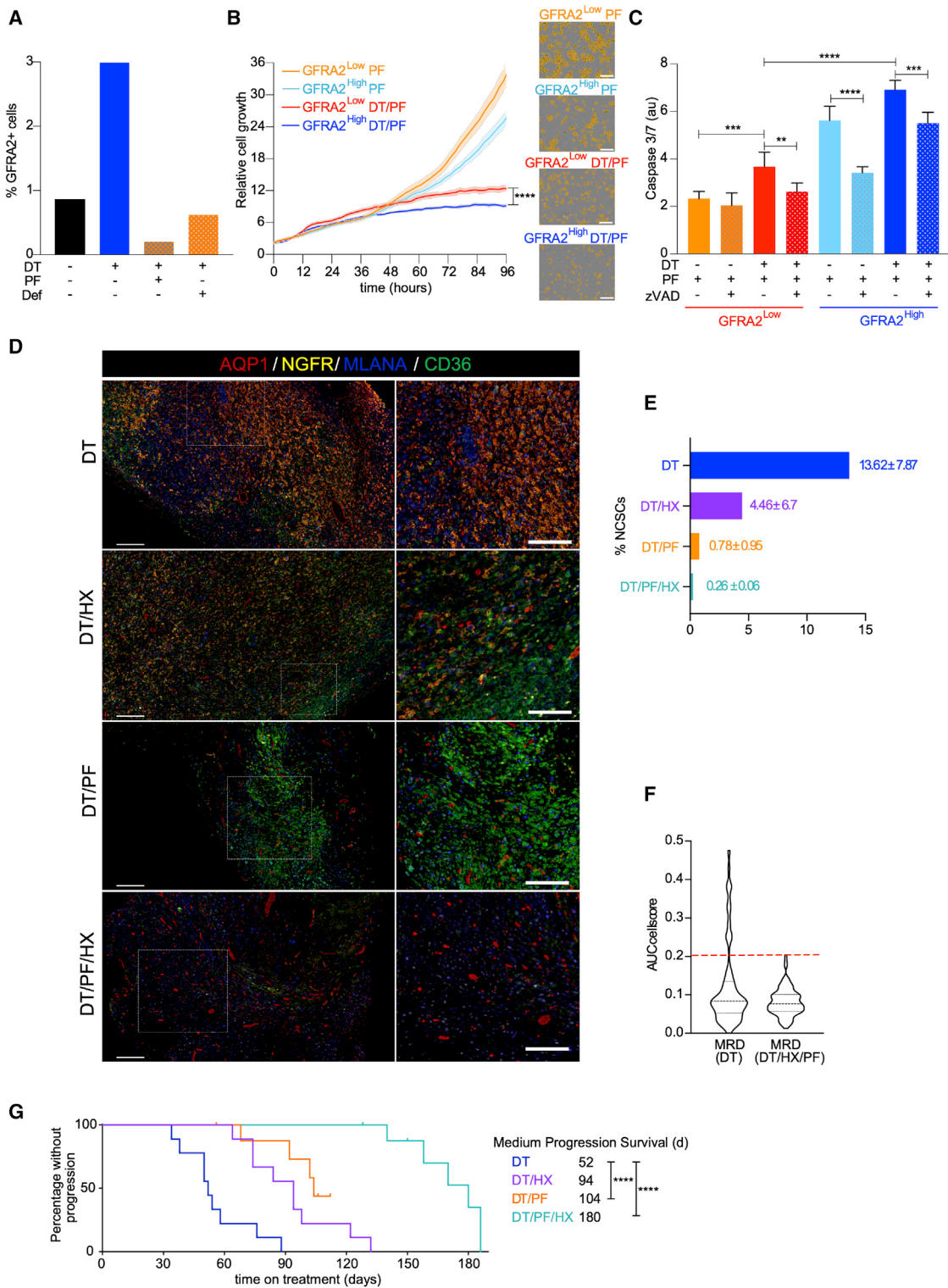


**Figure 4. Targeting the NCSCs delays the onset of therapy resistance**

(A) Percentage of MEL006 GFRA2+ cells quantified by flow cytometry after 48 h of exposure to the treatment. Experimental conditions: DT (40 nM/8 nM) alone or in combination with two FAK inhibitors; PF562271 (1  $\mu$ M) and defactenib (1  $\mu$ M). The experiment was performed more than three times. Data from one representative experiment are shown.

(B) Relative growth of GFRA2<sup>high</sup> (orange) and GFRA2<sup>low</sup> (blue) cells sorted by FACS from a parental culture of MM383 cells and exposed to a FAK inhibitor alone (1  $\mu$ M PF562271, PF) (light color) or in combination with BRAF/MEK inhibitors (40 nM dabrafenib, 8 nM trametinib, DT/PF) (dark color). Representative culture

(legend continued on next page)

test whether transition from drug tolerance to resistance depends on a particular cellular MRD composition. We subjected all resistant lesions to bulk targeted DNA sequencing analysis. While, as described above, we failed to identify resistance-conferring events in lesions that re-emerged under DT (0/10), resistance-conferring genetic alterations were identified in most (8/9) MEL006 lesions that acquired resistance to the DT/PF/HX combination (Figure 5A). One of these lesions (M6\_R\_DTHXPF\_04) carried an NRAS<sup>Q61K</sup> activating mutation, previously described to confer resistance to BRAF/MEK inhibition (Nazarian et al., 2010) (Figure S5A). BRAF amplification, a particularly common resistance-conferring event (Xue et al., 2017), was detected in most (7/9) DT/PF/HX-resistant lesions, but not in any of the T0 or DT-resistant lesions. A quantitative PCR DNA analysis confirmed the increase in *BRAF*, but not *CRAF*, copy number in those samples (M6\_R\_DTHXPF\_01, 02, 06, 08, and M6\_R\_DTHXPF\_09), but not in DT-resistant lesions analyzed (Figures 5B and S5C). The increase in *BRAF* copy number was further confirmed at single-cell resolution by DNA fluorescence *in situ* hybridization (FISH) (Figures 5C and S5B). This latter analysis showed that the vast majority of cells carried the *BRAF* gene amplification, consistent with a clonal cell population. We failed to detect a genetic cause of resistance in only one (M6\_R\_DTHXPF\_05) of the nine lesions analyzed. It remains unclear whether resistance in this case was driven by a genetic alteration that we did not screen for or through a nongenetic mechanism. A western blot analysis of this sample, as well as the *NRAS*-mutant (M6\_R\_DTHXPF\_04) and two *BRAF*-amplified samples (M6\_R\_DTHXPF\_02 and 06), showed a similarly dramatic elevation in p-ERK (and p-P38) levels (Figures 5D and 5E). In comparison, levels of p-ERK (and p-P38) were much lower in DT-resistant lesions (5/5), all of which exhibited increased p-AKT levels instead. Although more extensive genetic analysis is required to draw firm conclusions, this observation indicates that resistance in M6\_R\_DTHXPF\_05 might also have a genetic origin. More importantly, the data also raise the possibility that, whereas nongenetic drug resistance evolution may favor activation of AKT signaling, genetic mechanisms seemingly prioritize ERK reactivation.

We therefore reasoned that lesions that escaped the NCSC-directed therapy through acquisition of genetic alterations may be sensitive to ERK inhibition. Accordingly, exposure of cells from three different DT/HX/PF MEL006-resistant lesions to increasing concentrations of two different ERK inhibitors showed

that the resistant cells were far more sensitive than their matching control cells (Ctr; Figure 5F). This observation therefore provides a clinically viable approach for the treatment of patients that would progress on an NCSC-targeted therapy.

Notably, immunostaining demonstrated that the increase in p-ERK levels was homogeneously distributed among virtually all individual cells in DT/HX/PF-resistant tumors (but not DT-resistant tumors), again consistent with resistance being driven by a clonal genetic event in the DT/HX/PF-resistant lesions (Figures 5D and 5E). Because exposure to PF and HX eradicated emergence of DT-induced NCSCs (Figures 4C and 4D), these data indicated that the presence of the NCSC drug-tolerant subpopulation at MRD is required for the development of nongenetic resistance. Together, these data further establish a strict correlation between the presence of NCSCs at MRD and nongenetic therapy resistance.

## DISCUSSION

We have previously shown that transient de-differentiation of melanoma cells into an NCSC state contributes to the development of resistance to targeted therapy (Rambow et al., 2018). One of the key findings we report here is that the NCSCs rely on FAK signaling for growth and survival. This parallels a recent observation that a NCSC population, which contributes to jaw bone regeneration, gains activity within the FAK signaling cascade, and that inhibiting FAK abolishes new bone formation (Ransom et al., 2018). It is also related to another study, which reported increased FAK signaling in melanoma cells exposed to a BRAF inhibitor (Hirata et al., 2015). This study, however, reported that activation of FAK in melanoma cells is driven by a "paradoxical" activation of melanoma-associated fibroblasts, induction of matrix production, and remodeling, leading to elevated integrin  $\beta$ 1/FAK/Src signaling (Hirata et al., 2015). In contrast, we show here that therapy-induced FAK signaling in the NCSC population is caused by the activation of an autocrine loop in which GDNF, produced by the NCSCs themselves, engages GFRA2-dependent activation of FAK signaling and one of its downstream pro-survival targets, AKT. Interestingly, we also show that NCSCs can promote activation of the NCSC transcriptional program in a paracrine fashion, an observation that may, at least partly, explain why NCSCs tend to occur in geographically localized clusters in MRD lesions (Rambow et al., 2018). The molecular mechanisms underlying this paracrine effect remain to be elucidated. GDNF, which is produced

regions of interest at a 96 h time point. Scale bars, 300  $\mu$ m. The analysis was performed using the IncuCyte live imager. Data ( $n = 6$ ) shows mean (thick line)  $\pm$  SEM (filled area). Unpaired t test; \*\*\*\*p < 0.0001.

(C) Caspase-3/7 activity in cultures of GFRA2<sup>high</sup> (orange) and GFRA2<sup>low</sup> (blue) cells sorted by FACS from an MM383 cell culture and exposed to a FAK inhibitor alone (1  $\mu$ M PF562271, PF) (light color) or in combination with BRAF/MEK inhibitors (40 nM dabrafenib, 8 nM trametinib, DT/PF) (dark color) and a pan-caspase inhibitor, zVAD (50 mM) (polka dot pattern). Data show mean of biological replicates ( $n = 6$ )  $\pm$  SD. Unpaired t test; \*\*p < 0.01, \*\*\*p < 0.001, \*\*\*\*p < 0.0001.

(D) Multiplex immunostaining for AQP1 (red), NGFR (yellow), MLANA (blue), and CD36 (green) in MRD following combination treatment with DT, an RXR antagonist (HX), and focal adhesion kinase inhibitor (PF).

(E) Quantification of AQP1/NGFR-double-positive NCSCs from multiplex immunostaining. The frequency of NGFR/AQP1-double-positive cells are indicated as percentage per area  $\pm$  SEM ( $n = 3$  biological replicates; 3 areas per sample). Scale bars, 200  $\mu$ m.

(F) Comparison of the cellular composition of MRD from MEL006 lesions treated with DT versus DT/HX/PF using single-cell RNA sequencing. The NCSC activity per cell was inferred using AUCell (Albar et al., 2017). NCSCs were detected from DT, but not DT/PF/HX, MRD (AUCell score < 0.2).

(G) Kaplan-Meier curve for MEL006 mice treated with DT alone ( $n = 9$ ) (Rambow et al., 2018), DT plus HX531 (DT/HX,  $n = 9$ ) (Rambow et al., 2018), DT plus FAK inhibitor, PF562271 (DT/PF,  $n = 9$ ), and the quadruple combination (DT/PF/HX). Median time to progression was 52 days for DT, 94 days for DT/HX, 104 days for DT/PF, and 180 days for DT/PF/HX. Log rank (Mantel-Cox) for DT versus DT/PF: \*\*\*\*p < 0.0001; and DT versus DT/PF/HX: \*\*\*\*p < 0.0001.

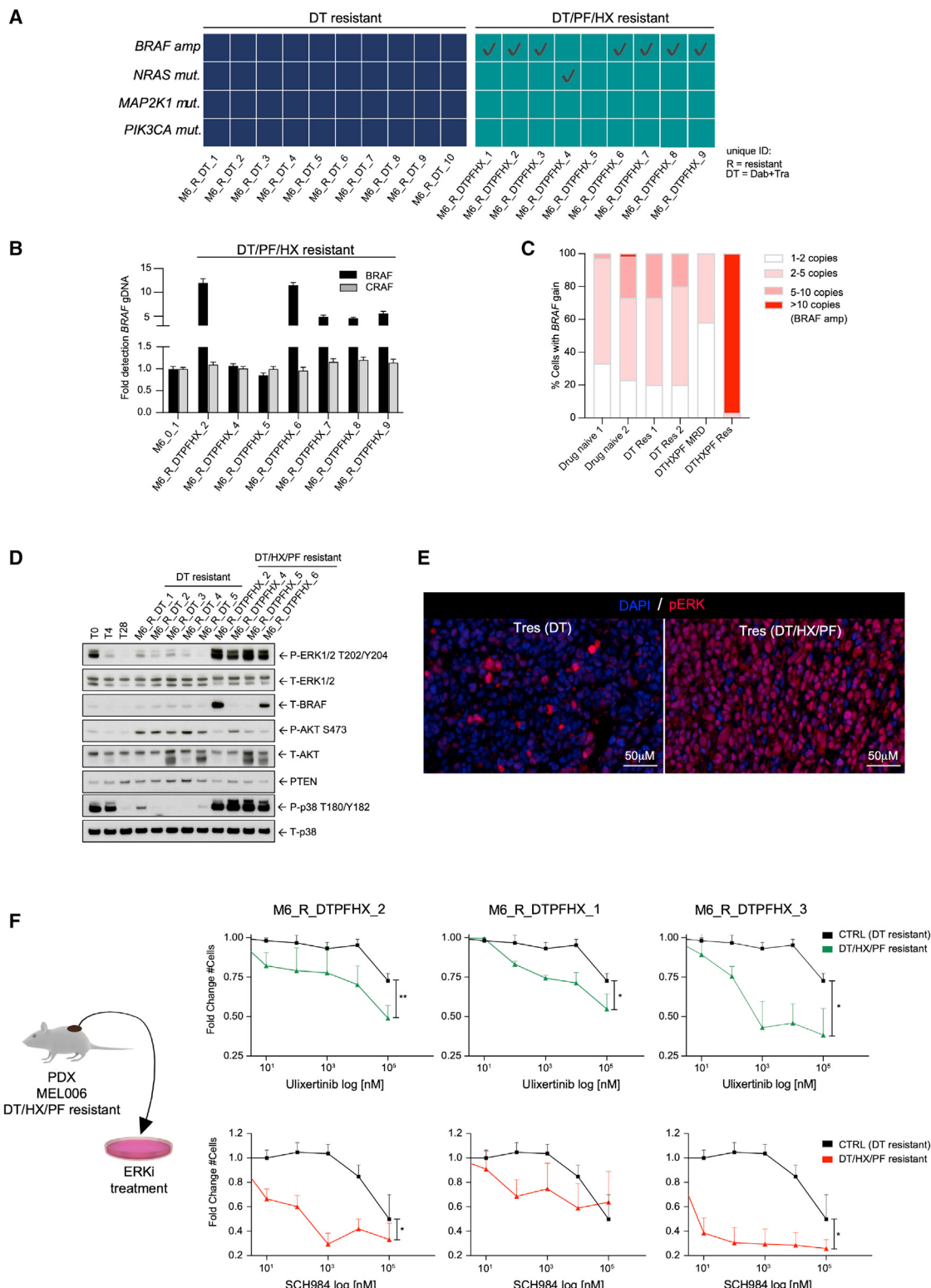


**Figure 5. Targeting the NCSCs prevents nongenetic drug resistance evolution**

(A) Interrogation of known genetic driver events of BRAFi&MEKi resistance, including BRAF-mutant splicing variants, in MEL006 lesions that acquired resistance to DT or DT/PF/HX lesions using both targeted DNA sequencing and RT-PCR approaches.

(B) Quantitative PCR analysis for *BRAF* and *CRAF* copy number was performed from genomic DNA. RQ = relative number of copies compared with T0. Mean ± SD of an n = 3 technical replicate.

(legend continued on next page)

by the NCSCs, may act as an inducer of phenotypic conversion into an NCSC state through its ability to induce signaling independently of GFRalpha, for example, via the RET or MET receptors (Ibanez et al., 2020). These receptors are indeed expressed in melanoma cells, including those that do not harbor an NCSC state, and their activation by GDNF may indeed initiate such a phenotypic switch. In keeping, GDNF was shown to contribute to paracrine regulation in a multitude of biological processes, such as, for example, spermatogonial self-renewal and differentiation (Meng et al., 2000). It will therefore be interesting to test whether GDNF (or other factors) secreted by the NCSCs is a key trigger of this paracrine effect.

The observation that NCSCs rely on FAK signaling has several important clinical implications. We show that exposure to FAK inhibitors strongly decreases emergence of the NCSCs in MRD lesions, and drastically delays the onset of resistance to RAF/MEK inhibitors in preclinical PDX models. Moreover, we show that, although emergence of the NCSC population in MRD is strongly compromised upon FAK inhibition, it can only be fully abolished by combining PF with HX, an RXR antagonist. Accordingly, this regimen produced a significantly longer median PFS period than the DT/PF combination and delayed the development of resistance even further. Note that this treatment did not cause any relevant adverse reaction or weight loss in PDXs. Our study therefore provides a strong rationale for the testing of the DT/PF and DT/PF/HX combinations in BRAF<sup>V600E</sup>-mutant melanoma patients.

Importantly, de-differentiation into an NCSC-like state was also reported as an escape mechanism to T cell transfer therapy (Boshuizen et al., 2020; Landsberg et al., 2012; Mehta et al., 2018). This can be explained by the drastic decrease of expression of melanoma antigens, including MART1/gp100, as cells de-differentiate (Boiko et al., 2010; Civenni et al., 2011). Because NCSCs exhibit stem cell features, we had postulated that this subpopulation may also activate mechanisms allowing them to escape the immune defense and, thereby, provide a pool of cells that are refractory to immune checkpoint blockade (ICB) (Rambow et al., 2019). The presence of these cells in tumors before exposure to ICB or their accumulation during treatment may therefore contribute, respectively, to both intrinsic and adaptive resistance to immunotherapy. Together, these findings highlighted the urgent need for therapeutic strategies directed at this melanoma subpopulation and emphasized how large is the subset of melanoma patients that may benefit from (the above-described) NCSC-directed therapy.

Importantly, although pharmacological eradication of the NCSC population in PDXs was sufficient to avoid the development of nongenetic resistance it did not prevent relapse. Resistance eventually developed through acquisition of *de novo* resistance-conferring genetic alterations. The prediction from these experi-

ments is that, although useful to extend PFS, NCSC-directed therapies are unlikely to be curative. However, these experiments were conducted on an immunocompromised background (i.e., nude mice) and MRD lesions from mice exposed to the DT/PF/HX combination were almost exclusively composed of hyperdifferentiated melanoma cells. It remains possible that these cells may eventually be cleared by the immune system. Moreover, these cells are likely to be highly responsive to both T cell therapy or ICB. These data therefore also warrant the implementation into the clinic of a sequential treatment regimen in which tumor debulking is induced by the DT/PF/HX combination followed by an immunotherapy approach aiming at eradicating the residual pool of hyperdifferentiated cells.

It has been proposed that discrete subpopulations of cancer cells may harbor increased “epigenetic” plasticity that permits random activation of alternate gene-regulatory networks, thus allowing acquisition of specific phenotypic properties through nongenetic reprogramming (Flavahan et al., 2017). Some of these properties may be maintained through cell division, and eventually lead to the selection of drug-resistant “epiclones.” Consistently, the findings described here identify the NCSCs as a melanoma subpopulation that is highly permissive to nongenetic reprogramming and a key driver of nongenetic resistance. Interestingly, we also provide evidence that nongenetic resistance can develop in the absence of selection of a single, genetically distinct, clonal population, a conclusion that is further supported by the recent re-analysis of our single-cell data with Longitudinal Analysis of Cancer Evolution, an algorithm that processes single-cell somatic mutation profiles from scRNA-seq data (Ramazzotti et al., 2020). Together, these analyses raise the possibility that nongenetic resistance may not be clonal but develop, instead, through collective reprogramming.

The ability in PDX models to repeatedly treat the same tumor over and over again led to the key and rather unexpected finding that a given tumor recurrently selects either a genetic or nongenetic drug resistance trajectory. We provided evidence that nongenetic resistance only develops following emergence of the NCSCs in MRD. These data indicate that the cellular composition of MRD dictates whether resistance develops through a genetic or nongenetic mechanism and therefore that this process is deterministic and predictable. The clinical implications of this finding are far-reaching. For instance, whether a given patient will benefit from combination treatments that make use of epigenetic drugs (for which several clinical trials are ongoing) depends on the MRD composition. Given the inter-patient variability of the cellular composition of MRD, our data highlight the need to develop personalized MRD-targeting therapies. Note that the clinical implementation of such therapies will require the ability to access serial tumor samples and their deep analysis using, for instance,

(C) Quantification of percentage of cells exhibiting BRAF copy gain as assessed by DNA FISH analysis using Dual Color Break Apart Probe (ZytoVision) on PDX tissue sections from treatment-naïve lesions (T0) and lesions that acquired resistance to DT or DT/PF/HX.

(D) Western blot analysis of levels of ERK and AKT phosphorylation and BRAF protein expression in lysates from MEL06 PDX tumors before treatment (T0) and ON treatment with DT for 4 days (T4), at MRD (T28), and after the development of resistance to DT or DT/HX/PF.

(E) Representative immunofluorescence staining with anti-p-ERK antibodies (red) in resistant lesions that escaped the DT (TRes DT01 is shown) and DT/HX/PF (qTRes01 is shown) treatments. Slides were counterstained with DAPI (blue).

(F) Quantification of cell viability assay of MEL06 DT-resistant primary cells (CTRL) and primary cells derived from MEL06 DT/PF/HX-resistant lesions harboring BRAF gene amplification (M6\_R\_DTPFHX\_1, M6\_R\_DTPFHX\_2, and M6\_R\_DTPFHX\_3) treated with ERK inhibitors (ulixertinib, green and SCH984, red). Mean (n = 4); bars, SD; \*p < 0.05, \*\*p < 0.01.

emerging single-cell spatial multi-omics methods. Because access to ON treatment biopsies is often problematic in the context of solid cancers, such as melanoma, a possible future alternative will be the development of non-invasive and ultrasensitive methods able to capture cellular composition of MRD from liquid biopsies. We argue that priority should be given to these technological developments as they will likely lead to promising therapeutic avenues that negate the increasingly recognized contribution of nongenetic mechanisms to therapy resistance.

### STAR★METHODS

Detailed methods are provided in the online version of this paper and include the following:

- [KEY RESOURCES TABLE](#)
- [RESOURCES AVAILABILITY](#)
  - Lead contact
  - Materials availability
  - Data and code availability
- [EXPERIMENTAL MODEL AND SUBJECT DETAILS](#)
  - Patient derived xenograft samples
  - Cell lines
- [METHODS DETAILS](#)
  - Drugs
  - Tissue culture
  - Apoptosis assay
  - Western blotting
  - RT-qPCR
  - Patient-derived xenografts
  - Pharmacologic treatment of mice
  - Fluorescence *in situ* hybridization analysis
  - Immunofluorescence on PDX biopsies
  - Multiplexed, sequential immunohistochemistry and analysis
  - FACS
  - Single cell sorting and SMARTseq2 based scRNA sequencing
  - Targeted scDNA sequencing
  - Droplet based scRNA sequencing
  - Targeted bulk DNAseq
  - Copy number analysis
  - Whole-exome sequencing
  - Exome sequencing analysis
  - Stem and lineage score assessment
  - GDNF ELISA
  - Sanger sequencing
  - BRAF-splicing PCR
  - Meta-analysis of resistance mechanisms to MAPK inhibition
  - Meta-analysis of NCSC signature induction upon MAPK inhibition
  - Data availability
- [QUANTIFICATION AND STATISTICAL ANALYSIS](#)

### SUPPLEMENTAL INFORMATION

Supplemental information can be found online at <https://doi.org/10.1016/j.ccr.2021.05.015>.

### ACKNOWLEDGMENTS

We thank Prof. G. Ghanem, LOCE-Institut J. Bordet, Université Libre de Bruxelles for providing us with the MM lines. We thank Göran Jönsson (Lund University) for the MM383 and WM852 cell lines. We thank Odessa Van Goethem and the excellent staff of the KU Leuven PDX platform (TRACE) for their assistance with the PDX experiments. TRACE is supported by the Stichting Tegen Kanker grant 2016-054. E.L. is supported by the Melanoma Research Alliance (MRA) Amanda and Jonathan Lilian young investigator award. Flow cytometry/FACS was performed at the KU Leuven FACS Core Facility. Lukas Marcelis and Jasmin Garg provided histology support and help with mIHC, respectively. O.M.-B. is supported by 12T1217N project by FWO at the program under the Marie Skłodowska-Curie grant agreement no. 665501. P.K. received financial support from Marie Curie Individual Fellowship (H2020-MSCA-IF-2018), J.P. received financial support from Marie Curie Individual Fellowship (H2020-MSCA-IF-2019) and J.F. from the Swedish Research Council (Vetenskapsrådet, International postdoc grant, registration no. 2016-00215). J.D. is supported by a postdoctoral fellowship from FWO (12J6921N). D.P. and N.V.R. received PhD fellowships from the VIB PhD international program and FWO-SB 1S79619N, respectively. This work was supported by FWO (no. #G.0929.16N), Stichting Tegen Kanker, Interreg (Skin-Huid), Melanoma Research Alliance (MRA), (EIA#623591), KU Leuven (C1 grant no. #C16/19/006) to J.-C.M., an OHSU Knight Cancer Center support grant from the National Institutes of Health (NIH P30-CA069533) to A.W.L., infrastructure grants (type 1 funding from the Hercules Foundation—AKUL/13/41; Foundation Against Cancer project 2015-143) and grants from FWO (I001818N) and KU Leuven C14/18/092 to T.V. and enabled through access to the MRC eMedLab Medical Bioinformatics infrastructure, supported by the Medical Research Council (grant no. MR/L016311/1).

### AUTHOR CONTRIBUTIONS

F.R., O.M.-B., and A.R. designed and conducted the experiments, and acquired, analyzed, and interpreted the data. M.D., P.K., D.P., and N.V.R. conducted the experiments and acquired the data. M.D. and P.K. contributed to analysis and interpretation of the resulting data. E.L. provided help in setting up and interpreting the PDX experiments. J.P., J.D., D.L., and T.V. helped generate, and analyzed and interpreted the shallow WGS, WES, and SNP array data. G.B. conducted SMARTseq2 and qPCR experiments. O.B., F.B., M.P.L., H.R., and J.J.v.d.O. provided human samples and pathology support. I.Vd.B., S.L., and S.Vd.B. conducted DNA FISH BRAFamp analysis and targeted DNA sequencing data interpretation, respectively. J.F. conducted mIHC and A.W.L. interpreted the data. All authors read and edited the manuscript. F.R. and J.-C.M. conceptualized, designed research studies, and wrote the manuscript.

### DECLARATION OF INTEREST

The authors declare no competing interests.

J.-C.M. and F.R. are authors on a patent application related to this work.

Received: January 17, 2020

Revised: February 17, 2021

Accepted: May 20, 2021

Published: June 17, 2021

### REFERENCES

- Aibar, S., Gonzalez-Blas, C.B., Moerman, T., Huynh-Thu, V.A., Imrichova, H., Hulselmans, G., Rambow, F., Marine, J.C., Geurts, P., Aerts, J., et al. (2017). SCENIC: single-cell regulatory network inference and clustering. *Nat. Methods* 14, 1083–1086.
- Airaksinen, M.S., and Saarma, M. (2002). The GDNF family: signalling, biological functions and therapeutic value. *Nat. Rev. Neurosci.* 3, 383–394.
- Arozarena, I., and Wellbrock, C. (2019). Phenotype plasticity as enabler of melanoma progression and therapy resistance. *Nat. Rev. Cancer* 19, 377–391.
- Bell, C.C., Fennell, K.A., Chan, Y.C., Rambow, F., Yeung, M.M., Vassiliadis, D., Lara, L., Yeh, P., Martelotto, L.G., Rogiers, A., et al. (2019). Targeting enhancer

- switching overcomes non-genetic drug resistance in acute myeloid leukaemia. *Nat. Commun.* 10, 2723.
- Boiko, A.D., Razorenova, O.V., van de Rijn, M., Swetter, S.M., Johnson, D.L., Ly, D.P., Butler, P.D., Yang, G.P., Joshua, B., Kaplan, M.J., et al. (2010). Human melanoma-initiating cells express neural crest nerve growth factor receptor CD271. *Nature* 466, 133–137.
- Boshuizen, J., Vredevoogd, D.W., Krijgsman, O., Ligtenberg, M.A., Blankenstein, S., de Brujin, B., Frederick, D.T., Kenski, J.C.N., Parren, M., Bruggemann, M., et al. (2020). Reversal of pre-existing NGFR-driven tumor and immune therapy resistance. *Nat. Commun.* 11, 3946.
- Civenni, G., Walter, A., Kobert, N., Mihic-Probst, D., Zipser, M., Belloni, B., Seifert, B., Moch, H., Dummer, R., van den Broek, M., and Sommer, L. (2011). Human CD271-positive melanoma stem cells associated with metastasis establish tumor heterogeneity and long-term growth. *Cancer Res.* 71, 3098–3109.
- Dentro, S.C., Wedge, D.C., and Van Loo, P. (2017). Principles of reconstructing the subclonal architecture of cancers. *Cold Spring Harbor Perspect. Med.* 7, a026625.
- Fallahi-Sichani, M., Becker, V., Izar, B., Baker, G.J., Lin, J.R., Boswell, S.A., Shah, P., Rotem, A., Garraway, L.A., and Sorger, P.K. (2017). Adaptive resistance of melanoma cells to RAF inhibition via reversible induction of a slowly dividing de-differentiated state. *Mol. Syst. Biol.* 13, 905.
- Flavahan, W.A., Gaskell, E., and Bernstein, B.E. (2017). Epigenetic plasticity and the hallmarks of cancer. *Science* 357, eaal2380.
- Fong, C.Y., Gilan, O., Lam, E.Y., Rubin, A.F., Ftoni, S., Tyler, D., Stanley, K., Sinha, D., Yeh, P., Morison, J., et al. (2015). BET inhibitor resistance emerges from leukaemia stem cells. *Nature* 525, 538–542.
- Froyen, G., Le Mercier, M., Lierman, E., Vandepoele, K., Nollet, F., Boone, E., Van der Meulen, J., Jacobs, K., Lambin, S., Vander Borght, S., et al. (2019). Standardization of somatic variant classifications in solid and haematological tumours by a two-level approach of biological and clinical classes: an initiative of the Belgian ComPerMed expert panel. *Cancers* 11, 2030.
- Gori, K., and Baez-Ortega, A. (2018). sigfit: flexible Bayesian inference of mutational signatures. *bioRxiv*, 372896. <https://doi.org/10.1101/372896>.
- Hirata, E., Girotti, M.R., Viros, A., Hooper, S., Spencer-Dene, B., Matsuda, M., Larkin, J., Marais, R., and Sahai, E. (2015). Intravital imaging reveals how BRAF inhibition generates drug-tolerant microenvironments with high integrin beta1/FAK signaling. *Cancer Cell* 27, 574–588.
- Holohan, C., Van Schaeybroeck, S., Longley, D.B., and Johnston, P.G. (2013). Cancer drug resistance: an evolving paradigm. *Nat. Rev. Cancer* 13, 714–726.
- Hugo, W., Shi, H., Sun, L., Piva, M., Song, C., Kong, X., Moriceau, G., Hong, A., Dahlman, K.B., Johnson, D.B., et al. (2015). Non-genomic and immune evolution of melanoma acquiring MAPKi resistance. *Cell* 162, 1271–1285.
- Ibanez, C.F., Paratcha, G., and Ledda, F. (2020). RET-independent signaling by GDNF ligands and GFRalpha receptors. *Cell Tissue Res.* 382, 71–82.
- Khandelwal, G., Girotti, M.R., Smownton, C., Taylor, S., Wirth, C., Dynowski, M., Frese, K.K., Brady, G., Dive, C., Marais, R., and Miller, C. (2017). Next-generation sequencing analysis and algorithms for PDX and CDX models. *Mol. Cancer Res.* 15, 1012–1016.
- Kim, C., Gao, R., Sei, E., Brandt, R., Hartman, J., Hatschek, T., Crosetto, N., Foukakis, T., and Navin, N.E. (2018). Chemoresistance evolution in triple-negative breast cancer delineated by single-cell sequencing. *Cell* 173, 879–893.e813.
- Knoechel, B., Roderick, J.E., Williamson, K.E., Zhu, J., Lohr, J.G., Cotton, M.J., Gillespie, S.M., Fernandez, D., Ku, M., Wang, H., et al. (2014). An epigenetic mechanism of resistance to targeted therapy in T cell acute lymphoblastic leukemia. *Nat. Genet.* 46, 364–370.
- Kondo, A., Yamamoto, S., Nakaki, R., Shimamura, T., Hamakubo, T., Sakai, J., Kodama, T., Yoshida, T., Aburatani, H., and Osawa, T. (2017). Extracellular acidic pH activates the sterol regulatory element-binding protein 2 to promote tumor progression. *Cell Rep.* 18, 2228–2242.
- Kwong, L.N., Boland, G.M., Frederick, D.T., Helms, T.L., Akid, A.T., Miller, J.P., Jiang, S., Cooper, Z.A., Song, X., Seth, S., et al. (2015). Co-clinical assessment identifies patterns of BRAF inhibitor resistance in melanoma. *J. Clin. Invest.* 125, 1459–1470.
- Landsberg, J., Kohlmeyer, J., Renn, M., Bald, T., Rogava, M., Cron, M., Fatho, M., Lennerz, V., Wolfel, T., Holzel, M., and Tuting, T. (2012). Melanomas resist T-cell therapy through inflammation-induced reversible dedifferentiation. *Nature* 490, 412–416.
- Lee, G., Kim, H., Elkabetz, Y., Al Shamy, G., Panagiotakos, G., Barberi, T., Tabar, V., and Studer, L. (2007). Isolation and directed differentiation of neural crest stem cells derived from human embryonic stem cells. *Nat. Biotechnol.* 25, 1468–1475.
- Long, G.V., Fung, C., Menzies, A.M., Pupo, G.M., Carlino, M.S., Hyman, J., Shahheydari, H., Tembe, V., Thompson, J.F., Saw, R.P., et al. (2014). Increased MAPK reactivation in early resistance to dabrafenib/trametinib combination therapy of BRAF-mutant metastatic melanoma. *Nat. Commun.* 5, 5694.
- Luskin, M.R., Murakami, M.A., Manalis, S.R., and Weinstock, D.M. (2018). Targeting minimal residual disease: a path to cure? *Nat. Rev. Cancer* 18, 255–263.
- Marine, J.C., Dawson, S.J., and Dawson, M.A. (2020). Non-genetic mechanisms of therapeutic resistance in cancer. *Nat. Rev. Cancer* 20, 743–756.
- Mehta, A., Kim, Y.J., Robert, L., Tsui, J., Comin-Anduix, B., Berent-Maoz, B., Cochran, A.J., Economou, J.S., Tumeh, P.C., Puig-Saus, C., and Ribas, A. (2018). Immunotherapy resistance by inflammation-induced dedifferentiation. *Cancer Discov.* 8, 935–943.
- Meng, X., Lindahl, M., Hyvonen, M.E., Parvinen, M., de Rooij, D.G., Hess, M.W., Raatikainen-Ahokas, A., Sainio, K., Rauvala, H., Lakso, M., et al. (2000). Regulation of cell fate decision of undifferentiated spermatogonia by GDNF. *Science* 287, 1489–1493.
- Menon, D.R., Das, S., Krepler, C., Vultur, A., Rinner, B., Schauer, S., Kashofer, K., Wagner, K., Zhang, G., Rad, E.B., et al. (2015). A stress-induced early innate response causes multidrug tolerance in melanoma. *Oncogene* 34, 4545.
- Mousson, A., Sick, E., Carl, P., Dujardin, D., De Mey, J., and Ronde, P. (2018). Targeting focal adhesion kinase using inhibitors of protein-protein interactions. *Cancers* 10, 278.
- Nazarian, R., Shi, H., Wang, Q., Kong, X., Koya, R.C., Lee, H., Chen, Z., Lee, M.K., Attar, N., Sazegar, H., et al. (2010). Melanomas acquire resistance to B-RAF(V600E) inhibition by RTK or N-RAS upregulation. *Nature* 468, 973–977.
- Nik-Zainal, S., Van Loo, P., Wedge, D.C., Alexandrov, L.B., Greenman, C.D., Lau, K.W., Raine, K., Jones, D., Marshall, J., Ramakrishna, M., et al. (2012). The life history of 21 breast cancers. *Cell* 149, 994–1007.
- Paratcha, G., and Ledda, F. (2008). GDNF and GFRalpha: a versatile molecular complex for developing neurons. *Trends Neurosciences* 31, 384–391.
- Peretz, Y., Wu, H., Patel, S., Bellacosa, A., and Katz, R.A. (2015). Inhibitor of DNA binding 4 (ID4) is highly expressed in human melanoma tissues and may function to restrict normal differentiation of melanoma cells. *PLoS One* 10, e0116839.
- Pogrebniak, K.L., and Curtis, C. (2018). Harnessing tumor evolution to circumvent resistance. *Trends Genetics : TIG* 34, 639–651.
- Pupo, G.M., Boyd, S.C., Fung, C., Carlino, M.S., Menzies, A.M., Pedersen, B., Johansson, P., Hayward, N.K., Kefford, R.F., Scolyer, R.A., et al. (2017). Clinical significance of intronic variants in BRAF inhibitor resistant melanomas with altered BRAF transcript splicing. *Biomark Res.* 5, 17.
- Ramazzotti, D., Angaroni, F., Maspero, D., Ascolani, G., Castiglioni, I., Piazza, R., Antoniotti, M., and Graudenzi, A. (2020). Longitudinal cancer evolution from single cells. *bioRxiv*. <https://doi.org/10.1101/2020.01.14.906453>.
- Rambow, F., Job, B., Petit, V., Gesbert, F., Delmas, V., Seberg, H., Meurice, G., Van Otterloo, E., Dessen, P., Robert, C., et al. (2015). New functional signatures for understanding melanoma biology from tumor cell lineage-specific analysis. *Cell Rep.* 13, 840–853.
- Rambow, F., Marine, J.C., and Goding, C. (2019). Melanoma plasticity and phenotypic diversity: therapeutic barriers and opportunities. *Genes Dev.*
- Rambow, F., Rogiers, A., Marin-Bejar, O., Aibar, S., Femel, J., Dewaele, M., Karras, P., Brown, D., Chang, Y.H., Debiec-Rychter, M., et al. (2018).

- Toward minimal residual disease-directed therapy in melanoma. *Cell* 174, 843–855 e819.
- Ransom, R.C., Carter, A.C., Salhotra, A., Leavitt, T., Marecic, O., Murphy, M.P., Lopez, M.L., Wei, Y., Marshall, C.D., Shen, E.Z., et al. (2018). Mechanoresponsive stem cells acquire neural crest fate in jaw regeneration. *Nature* 563, 514–521.
- Rizos, H., Menzies, A.M., Pupo, G.M., Carlino, M.S., Fung, C., Hyman, J., Haydu, L.E., Mijatov, B., Becker, T.M., Boyd, S.C., et al. (2014). BRAF inhibitor resistance mechanisms in metastatic melanoma: spectrum and clinical impact. *Clin. Cancer Res.* 20, 1965–1977.
- Robert, C., Grob, J.J., Stroyakovskiy, D., Karaszewska, B., Hauschild, A., Levchenko, E., Chiarion Sileni, V., Schachter, J., Garbe, C., Bondarenko, I., et al. (2019). Five-year outcomes with dabrafenib plus trametinib in metastatic melanoma. *N. Engl. J. Med.* 381, 626–636.
- Roesch, A., Vultur, A., Bogeski, I., Wang, H., Zimmermann, K.M., Speicher, D., Korbel, C., Laschke, M.W., Gimotty, P.A., Philipp, S.E., et al. (2013). Overcoming intrinsic multidrug resistance in melanoma by blocking the mitochondrial respiratory chain of slow-cycling JARID1B(high) cells. *Cancer Cell* 23, 811–825.
- Rogiers, A., Thomas, D., Vander Borght, S., van den Oord, J.J., Bechter, O., Dewaele, M., Rambow, F., Marine, J.C., and Wolter, P. (2019). Dabrafenib plus trametinib in BRAF K601E-mutant melanoma. *Br. J. Dermatol.* 180, 421–422.
- Schober, M., and Fuchs, E. (2011). Tumor-initiating stem cells of squamous cell carcinomas and their control by TGF-beta and integrin/focal adhesion kinase (FAK) signaling. *Proc. Natl. Acad. Sci. U S A* 108, 10544–10549.
- Shaffer, S.M., Dunagin, M.C., Torborg, S.R., Torre, E.A., Emert, B., Krepler, C., Begiri, M., Sproesser, K., Brifford, P.A., Xiao, M., et al. (2017). Rare cell variability and drug-induced reprogramming as a mode of cancer drug resistance. *Nature* 546, 431–435.
- Sharma, S.V., Lee, D.Y., Li, B., Quinlan, M.P., Takahashi, F., Maheswaran, S., McDermott, U., Azizian, N., Zou, L., Fischbach, M.A., et al. (2010). A chromatin-mediated reversible drug-tolerant state in cancer cell subpopulations. *Cell* 141, 69–80.
- Shi, H., Hugo, W., Kong, X., Hong, A., Koya, R.C., Moriceau, G., Chodon, T., Guo, R., Johnson, D.B., Dahlman, K.B., et al. (2014). Acquired resistance and clonal evolution in melanoma during BRAF inhibitor therapy. *Cancer Discov.* 4, 80–93.
- Shlush, L.I., Mitchell, A., Heisler, L., Abelson, S., Ng, S.W.K., Trotman-Grant, A., Medeiros, J.J.F., Rao-Bhatia, A., Jaciw-Zurakowsky, I., Marke, R., et al. (2017). Tracing the origins of relapse in acute myeloid leukaemia to stem cells. *Nature* 547, 104–108.
- Spagnolo, F., Ghiorzo, P., and Queirolo, P. (2014). Overcoming resistance to BRAF inhibition in BRAF-mutated metastatic melanoma. *Oncotarget* 5, 10206–10221.
- Stuart, T., Butler, A., Hoffman, P., Hafemeister, C., Papalexi, E., Mauck, W.M., 3rd, Hao, Y., Stoeckius, M., Smibert, P., and Satija, R. (2019). Comprehensive integration of single-cell data. *Cell* 177, 1888–1902. <https://doi.org/10.1016/j.cell.2019.05.031>.
- Su, Y., Wei, W., Robert, L., Xue, M., Tsoi, J., Garcia-Diaz, A., Homet Moreno, B., Kim, J., Ng, R.H., Lee, J.W., et al. (2017). Single-cell analysis resolves the cell state transition and signaling dynamics associated with melanoma drug-induced resistance. *Proc. Natl. Acad. Sci. U S A* 114, 13679–13684.
- Subramanian, A., Tamayo, P., Mootha, V.K., Mukherjee, S., Ebert, B.L., Gillette, M.A., Paulovich, A., Pomeroy, S.L., Golub, T.R., Lander, E.S., and Mesirov, J.P. (2005). Gene set enrichment analysis: a knowledge-based approach for interpreting genome-wide expression profiles. *Proc. Natl. Acad. Sci. U S A* 102, 15545–15550.
- Tai, Y.L., Chen, L.C., and Shen, T.L. (2015). Emerging roles of focal adhesion kinase in cancer. *Biomed. Research Int.* 2015, 690690.
- Trapnell, C., Cacchiarelli, D., Grimsby, J., Pokharel, P., Li, S., Morse, M., Lennon, N.J., Livak, K.J., Mikkelsen, T.S., and Rinn, J.L. (2014). The dynamics and regulators of cell fate decisions are revealed by pseudotemporal ordering of single cells. *Nat Biotechnol* 32, 381–386. <https://doi.org/10.1038/nbt.2859>.
- Trumpp, A., and Wiestler, O.D. (2008). Mechanisms of disease: cancer stem cells—targeting the evil twin. *Nat. Clin. Pract. Oncol.* 5, 337–347.
- Tsoi, J., Robert, L., Paraiso, K., Galvan, C., Sheu, K.M., Lay, J., Wong, D.J.L., Atefi, M., Shirazi, R., Wang, X., et al. (2018). Multi-stage differentiation defines melanoma subtypes with differential vulnerability to drug-induced iron-dependent oxidative stress. *Cancer cell* 33, 890–904.e5.
- Tsujikawa, T., Kumar, S., Borkar, R.N., Azimi, V., Thibault, G., Chang, Y.H., Balter, A., Kawashima, R., Choe, G., Sauer, D., et al. (2017). Quantitative multiplex immunohistochemistry reveals myeloid-inflamed tumor-immune complexity associated with poor prognosis. *Cell Rep.* 19, 203–217.
- Van der Auwera, G.A., and O'Connor, B.D. (2020). Genomics in the Cloud (O'Reilly Media, Inc.).
- Van Loo, P., Nordgard, S.H., Lingjaerde, O.C., Russnes, H.G., Rye, I.H., Sun, W., Weigman, V.J., Marynen, P., Zetterberg, A., Naume, B., et al. (2010). Allele-specific copy number analysis of tumors. *Proc. Natl. Acad. Sci. U S A* 107, 16910–16915.
- Vanden Bempt, I., Vander Borght, S., Sciot, R., Spans, L., Claerhout, S., Brems, H., Lehnert, S., Dehaspe, L., Fransis, S., Neuville, B., et al. (2021). Comprehensive targeted next-generation sequencing approach in the molecular diagnosis of gastrointestinal stromal tumor. *Genes Chromosomes Cancer* 60, 239–249.
- Williams, M.J., Werner, B., Heide, T., Curtis, C., Barnes, C.P., Sotoriva, A., and Graham, T.A. (2018). Quantification of subclonal selection in cancer from bulk sequencing data. *Nat. Genet.* 50, 895–903.
- Woolston, A., Khan, K., Spain, G., Barber, L.J., Griffiths, B., Gonzalez-Exposito, R., Hornsteiner, L., Punta, M., Patil, Y., Newey, A., et al. (2019). Genomic and transcriptomic determinants of therapy resistance and immune landscape evolution during anti-EGFR treatment in colorectal cancer. *Cancer Cell* 36, 35–50 e39.
- Xue, Y., Martelotto, L., Baslan, T., Vides, A., Solomon, M., Mai, T.T., Chaudhary, N., Riely, G.J., Li, B.T., Scott, K., et al. (2017). An approach to suppress the evolution of resistance in BRAFV600E-mutant cancer. *Nat. Med.* 23, 929–937.

## STAR★METHODS

## KEY RESOURCES TABLE

REAGENT or RESOURCE	SOURCE	IDENTIFIER
<b>Antibodies</b>		
Rabbit polyclonal anti-pERK	Cell Signaling	Cat#4370; RRID: AB_2315112
Rabbit polyclonal anti-ERK	Cell signaling	Cat#9102; RRID: AB_330744
Rabbit polyclonal anti-NGFR	Cell Signaling	Cat#8238; RRID: AB_10839265
Rabbit polyclonal anti-AQP1	Millipore	Cat#AB2219; RRID: AB_1163380
Goat polyclonal anti-GFRA2	R&D	Cat#AF429; RRID: AB_2294621
Goat polyclonal anti-MITF	R&D	Cat#AF5769; RRID: AB_2235141
Rabbit polyclonal anti-CD36	Sigma-Aldrich	Cat#HPA002018; RRID: AB_1078464
Rabbit polyclonal anti-MITF	Sigma-Aldrich	Cat#HPA003259; RRID: AB_1079381
Rabbit polyclonal anti-pFAK (Tyr397)	Genetex	Cat# GTX129840; RRID: AB_2886103
Rabbit polyclonal anti-pFAK (Tyr925)	Cell Signaling	Cat#3284; RRID: AB_10831810
Rabbit monoclonal anti-FAK	Cell Signaling	Cat#13009; RRID: AB_2798086
Rabbit monoclonal anti-AKT(Ser473)	Cell Signaling	Cat#4060; RRID: AB_2315049
Mouse monoclonal anti AKT (pan)	Cell Signaling	Cat#2920; RRID: AB_1147620
Rabbit polyclonal anti-MLANA	Sigma-Aldrich	Cat#HPA048662; RRID: AB_2680485
Rabbit monoclonal anti-SRC	Cell Signaling	Cat#2123; RRID: AB_2106047
Rabbit monoclonal anti-pSRC(Tyr416)	Cell signaling	Cat#6943; RRID: AB_10013641
Rabbit monoclonal anti-PTEN	Cell Signaling	Cat#9559; RRID: AB_390810
Rabbit monoclonal anti-P38 MAPK	Cell Signaling	Cat#8690; RRID: AB_10999090
Rabbit monoclonal anti-pP38 MAPK (Thr180/Tyr182)	Cell Signaling	Cat#4511; RRID: AB_2139682
Donkey anti-goat Alexa Fluor 594	Thermo Fisher Scientific	Cat#A-11058; RRID: AB_2534105
Donkey anti-rabbit Alexa Fluor 488	Thermo Fisher Scientific	Cat#A-21206; RRID: AB_2535792
Donkey Anti-Rabbit IgG Unconjugated	Jackson Immunoresearch	Cat#711-007-003; RRID: AB_2340587
Donkey anti-rabbit Fab fragment Alexa Fluor 488	Jackson Immunoresearch	Cat#111-547-003; RRID: AB_2338058
<b>Bacterial and virus strains</b>		
dsRed encoding viral vector, pHRSINcPPT-SGW RFP (VSV-G typed lentivirus, packed with third generation packaging constructs)	Laboratory for Translational Research in Gastrointestinal Disorders	N/A
<b>Biological samples</b>		
Patient biopsies	University of Zürich Hospital	<a href="http://www.en.usz.ch/Pages/default.aspx">http://www.en.usz.ch/Pages/default.aspx</a>
Patient-derived xenografts (PDXs)	KU Leuven	<a href="https://www.uzleuven-kuleuven.be/lki/trace/">https://www.uzleuven-kuleuven.be/lki/trace/</a>
<b>Chemicals, peptides, and recombinant proteins</b>		
Agencourt AMPure XP beads	Agencourt/ Beckman Coulter	Cat#A63881
Opti-MEM	GIBCO	Cat#21985-070
PBS	SIGMA	D8537
Matrigel	Corning	Cat#356253
TransIT-X2	Mirus	MIR6004
Dabrafenib	MCE	Cat#HY-14660
Trametinib	MCE	Cat#HY-10999
Normal Donkey Serum	Jackson Immunoresearch	Cat#017-000-121
Liberase	Sigma-Aldrich	Cat# 5401119001

(Continued on next page)

**Continued**

REAGENT or RESOURCE	SOURCE	IDENTIFIER
KAPA HiFi Hot start Readymix	Sopachem	Cat#KK2602
Superscript II	Thermo Fisher Scientific	Cat#10328062
Trypsin (0.25%)	Thermo Fisher Scientific	Cat#25200056
DAPI (4',6-Diamidino-2-Phenylindole, Dilactate)	Thermo Fisher Scientific	Cat#D3571
HX531	Tocris	Cat#3912
F-10 Nut Mix (Ham)	GIBCO	Cat#22390-025
RPMI Medium 1640	GIBCO	Cat#61870-010
FBS	GIBCO	Cat#10270-106
GlutaMAX	GIBCO	Cat#35050-038
Amphotericin B	GIBCO	Cat#15290-018
Penicillin/streptomycin	GIBCO	Cat#15140-122
Trypan Blue	Sigma Aldrich	Cat#T10282
Vectashield Antifade Mounting Medium	Vector Labs	Cat#H-1000
XCE2-SG probe	MetaSystems	Cat#D-0802-050-FI
<b>Critical commercial assays</b>		
Nextera XT library Prep Kit	Illumina	Cat#FC-131-1096
Nextera XT Index Kit v2 Set A	Illumina	Cat#FC-131-2001
Nextera XT Index Kit v2 Set B	Illumina	Cat#FC-131-2002
Nextera XT Index Kit v2 Set C	Illumina	Cat#FC-131-2003
Nextera XT Index Kit v2 Set D	Illumina	Cat#FC-131-2004
Chromium Single Cell A Chip	10x genomics	Cat#120236
Chromium i7 Multiplex kit	10x genomics	Cat#120262
Chromium Single Cell 3' Library & Gel Bead Kit v2	10x genomics	Cat#120237
ImmPress HRP Anti-Rabbit Ig (Peroxidase)	Vector Labs	Cat#MP-7401
ImmPress HRP Anti-Goat Ig (Peroxidase)	Vector Labs	Cat#MP-7405
AEC Peroxidase substrate kit	Vector Labs	Cat#SK-4200
Click-iT Plus EdU Alexa Fluor 647 Flow Cytometry Assay Kit	Thermo Fisher Scientific	Cat#C10634
<b>Deposited data</b>		
Raw data (scRNASeq, WES, SNParay and Trusight targeted DNAsequencing)	European Genome Archive	EGA: EGAS00001005314
<b>Experimental models: Cell lines</b>		
MM099	Prof. G. Ghanem, LOCE-institut J. Bordet, Université Libre de Bruxelles	N/A
Mel006	Primary cell Line derived from PDX model	N/A
MM383	Prof. G. Jönsson Lund University	N/A
WM852	Prof. G. Jönsson Lund University	N/A
<b>Experimental models: Organisms/strains</b>		
NMRI nude BomTac:NMRI- <i>Foxn1<sup>nude</sup></i>	Taconic	<a href="https://www.taconic.com/mouse-model/nmri-nude">https://www.taconic.com/mouse-model/nmri-nude</a>
<b>Oligonucleotides</b>		
Primers for alternatively spliced BRAF: F-GGCTCTCGGTATAAGATGGC	Long et al., 2014	N/A
Primers for alternatively spliced BRAF: R-ACAGGAAACGCACCATATCC	Long et al., 2014	N/A
ON-TARGETplus Non-targeting pool	Horizon Discovery (Dharmacon)	Cat# D-001810-10-20
SMARTpool: ON-TARGETplus PTK2 siRNA	Horizon Discovery (Dharmacon)	Cat#L-003164-00-0005

(Continued on next page)

**Continued**

REAGENT or RESOURCE	SOURCE	IDENTIFIER
ON-TARGETplus GFRA1 siRNA	Horizon Discovery (Dharmacon)	Cat#L-007913-00-0005
ON-TARGETplus SMARTpool Human GDNF	Horizon Discovery (Dharmacon)	Cat#L-011040-00-0005
SMARTpool Human GFRA2	Horizon Discovery (Dharmacon)	Cat#L-007914-00-0005
<b>Software and algorithms</b>		
Seurat (3.2.3)	Stuart et al., 2019	<a href="https://github.com/satijalab/seurat/releases">https://github.com/satijalab/seurat/releases</a>
AUCell (1.8.0)	Aibar et al., 2017	<a href="https://github.com/aertslab/AUCell">https://github.com/aertslab/AUCell</a>
Monocle (2.14.0)	Trapnell et al., 2014	<a href="https://www.bioconductor.org/packages/release/bioc/html/monocle.html">https://www.bioconductor.org/packages/release/bioc/html/monocle.html</a>
GSEA (4.1.0)	Subramanian et al. 2005	<a href="https://www.gsea-msigdb.org/gsea/index.jsp">https://www.gsea-msigdb.org/gsea/index.jsp</a>
GraphPad Prism 9	GraphPad Software	<a href="https://www.graphpad.com/scientific-software/prism/">https://www.graphpad.com/scientific-software/prism/</a>
R 3.6.1	R Project	<a href="https://www.r-project.org/">https://www.r-project.org/</a>
Cell Ranger R Kit	10x Genomics	<a href="https://support.10xgenomics.com/single-cell-gene-expression/software/pipelines/latest/rkit">https://support.10xgenomics.com/single-cell-gene-expression/software/pipelines/latest/rkit</a>
BWA mem (0.7.15-r1140, bwakit), Bamcmp (5cb0176)	Khandelwal et al., 2017	<a href="https://github.com/lh3/bwa/tree/master/bwakit">https://github.com/lh3/bwa/tree/master/bwakit</a>
GATK (v4.1.2.0)	Van der Auwera and O'Connor, 2020	<a href="https://github.com/broadinstitute/gatk/releases">https://github.com/broadinstitute/gatk/releases</a>
ASCAT (v2.5.2)	Van Loo et al., 2010	<a href="https://github.com/VanLoo-lab/ascat/releases">https://github.com/VanLoo-lab/ascat/releases</a>

**RESOURCES AVAILABILITY****Lead contact**

Further information and requests for resources and reagents should be directed to and will be fulfilled by the Lead Contact, Jean-Christophe Marine ([jeanchristophe.marine@kuleuven.be](mailto:jeanchristophe.marine@kuleuven.be))

**Materials availability**

All unique/stable reagents generated in this study are available from the Lead Contact with a completed Materials Transfer Agreement.

**Data and code availability**

Raw sequencing data of scRNAseq, WES, SNParray and targeted DNAseq (Trusight) are deposited to EGA under the accession number EGA: EGAS00001005314. Processed count matrices (scRNAsq) are available at: <https://marinelab.sites.vib.be/en>. No new code was generated for this study. Computational pipelines and associated used code are listed in Software and algorithms section.

**EXPERIMENTAL MODEL AND SUBJECT DETAILS****Patient derived xenograft samples**

Our cohort consisted of BRAF-mutant PDX melanoma models, treatment-naïve and BRAF/MEKi-treated samples. A summary of the genetic background of the PDX samples can be found in [Figure 2D](#).

**Cell lines**

The MEL06 and MEL015 primary cell lines were collected from the respective PDX models. UKE-1 cells were maintained in 5% CO2 at 37°C in F10 supplemented with 10% FBS, 0.25% GlutaMAX and Penicilline/Streptomycin antibiotics.

### METHODS DETAILS

#### Drugs

BRAFi Dabrafenib, MEKi Trametinib and FAKi PF562271 were purchased from MedChemExpress, RXR antagonist HX531 from Tocris, siRNA SMARTpools from Dharmacon (siRNA sequences are available upon request), recombinant GDNF from Peprotech.

#### Tissue culture

Cells from dissociated MEL006 tumours and MM099 short culture melanoma cells were grown in 5% CO<sub>2</sub> at 37°C in F10 supplemented with 10% FBS, 0.25% GlutaMAX and Penicilline/Streptomycin antibiotics. MM383 and WM852 cells were grown in 5% CO<sub>2</sub> at 37°C in RPMI GlutaMAX supplemented with 10% FBS and Penicilline/Streptomycin antibiotics.

#### Apoptosis assay

IncuCyte® Caspase-3/7 Red Apoptosis Assay Reagent (#4704) were used to measure apoptosis on an IncuCyte ZOOM system (Essen BioScience). The red fluorescence of 500 seeded cells on 96-well plate (TPP) were automated measured on pictures taken at 2 h intervals for the duration of the experiments.

#### Western blotting

Harvested cell culture pellets were resuspended in protein lysis buffer (25mM HEPES pH 7.5; 0.3M NaCl; 1,5mM MgCl<sub>2</sub>; 2mM EDTA; 2mM EGTA; 1mM DTT; 1% Triton X-100; 10% Glycerol; phosphatase/protease inhibitor cocktail), incubated on ice (15min) and centrifuged (15min) at 4°C/13000 rpm. Tumour samples were additionally homogenized with a PreCelllys in protein lysis buffer, prior to incubation on ice. Equal amounts of protein (Bradford quantification) were run on 4-12% Bis-Tris Plus Bolt gels (ThermoFisherScientific) and transferred to a nitrocellulose membrane with an iBlot dryblot system (ThermoFisherScientific). Membrane blocking (5% BSA/TBS-0,2%Tween) is followed by incubation with the appropriate primary antibodies and HRP-conjugated secondary antibody (Cell Signaling). Signals were detected by enhanced chemiluminescence (ThermoFisherScientific) on Amersham hyperfilm. Antibodies were from Cell Signaling Technology (P-FAK Y397, #8556; FAK, #13009; P-SRC Y416, #6943; SRC, #2123; P-AKT S473, #4060; AKT, #4691; P-ERK T202/Y204, #9106 (cell lines); P-ERK T202/Y204 #4370 (tumour lysates); ERK, #9102; BRAF, #9433; P-p38 T180/Y182, #4511; p38, #8690; PTEN, #9559)

#### RT-qPCR

Cells were harvested and mRNA extracted using the RNA NucleoSpin extraction kit (Macherey&Nagel). RNA was quantified using a NanoDrop 1000 (Thermo Scientific) and 500–2,000 ng was reverse transcribed with a High-Capacity cDNA Reverse Transcription Kit (ThermoFisherScientific). qPCRs were run using SensiFAST SYBR No-ROX Kit (Bioline) and a Roche LightCycler 384. Data processing with qbase+ 3.1 software (Biogazelle) relies on normalization with a minimum of 2 reference genes. RT-qPCR primer sequences are available upon request.

#### Patient-derived xenografts

In collaboration with TRACE, patient-derived xenografts (PDX) models were established using tissue from patients undergoing surgery as part of standard-of-care melanoma treatment at the University Hospitals KU Leuven. Written informed consent was obtained from all patients and all procedures involving human samples were approved by the UZ Leuven Medical Ethical Committee (S54185/S57760/S59199) and carried out in accordance with the principles of the Declaration of Helsinki. All procedures involving animals were performed in accordance with the guidelines of the IACUC and KU Leuven and were carried out within the context of approved project applications P038/2015, P098/2015 and P035/2016. Fresh tumour tissue was collected in transport medium (RPMI1640 medium supplemented with penicillin/streptomycin and amphotericin B). Tumour fragments were subsequently rinsed in phosphate-buffered saline supplemented with penicillin/streptomycin and amphotericin B and cut into small pieces of approximately 3 × 3 × 3 mm<sup>3</sup>. Tumour pieces were implanted subcutaneously in the interscapular fat pad of female SCID-beige mice (Taconic). Sedation and analgesia were performed using ketamine, medetomidine and buprenorphine. After reaching generation 4 (F4), one mouse with a tumour of 1000 mm<sup>3</sup> was sacrificed. This tumour was minced followed by dissociation using collagenase I & IV and trypsin. Cells were resuspended in serum-free DMEM/F12 medium and 250 000 cells were injected in the interscapular fat pad of 8 – 16 week-old female NMRI nude mice (Taconic). For single cell RNA sequencing purposes, cells were transduced with a lentivirus carrying dsRed. Cells were washed four times before injecting into the interscapular fat pad. For immunohistochemistry, non-dsRed-transduced lesions were used. For FACS, tumours were enzymatically dissociated using the same protocol.

#### Pharmacologic treatment of mice

Mice harboring tumours of a comparable size, ranging from 900 to 1000 mm<sup>3</sup>, were exposed to the BRAF-MEK combination via daily oral gavage. BRAF inhibitor dabrafenib and MEK inhibitor trametinib were dissolved in DMSO at a concentration of 30 and 0.3 mg/mL respectively, aliquoted and stored at -80°C. Each day a fresh aliquot was thawed and diluted 1:10 with phosphate-buffered saline. Mice were treated with a capped dose of 600 – 6 µg dabrafenib – trametinib respectively in 200 µL total volume. For the dabrafenib-trametinib-HX531 and dabrafenib-trametenib-PF562271 preparation, HX531 at 10 mg/dL and PF562271 at 45mg/mL

respectively in combination with dabrafenib and trametinib. Tumour volume was monitored with a caliper and the volume was calculated using the following formula:  $V = (\pi/6) \times \text{length} \times \text{width} \times \text{height}$ .

### Fluorescence *in situ* hybridization analysis

Interphase fluorescence *in situ* hybridization (FISH) was performed on 5-μm paraffin sections of formalin fixed (FFPE) xenograft tumour specimens applying the BRAF SPEC BRAF Dual Color Break Apart Probe (ZytoVision GmbH, Bremerhaven, Germany). In brief, FFPE sections were deparaffinized in three changes of xylenes, dehydrated in ethanol, pre-treated in sodium thiocyanate buffer (Abbott Molecular, Abbott Park, IL) for 30 minutes at 80°C, followed by pepsin digestion for 25 minutes at 37°C. Hybridization was performed at 37°C overnight. Slides were then washed and mounted with DAPI in an antifade solution. The number of fused BRAF signals was analyzed in 100 hundred successive, non-overlapping tumour cell nuclei using a Zeiss fluorescence microscope (Zeiss Axioplan, Oberkochen, Germany), controlled by Isis 5 software (Metasystems, Newton, MA).

### Immunofluorescence on PDX biopsies

Fluorescent staining was performed using OPAL staining reagents, which use individual tyramide signal amplification (TSA)-conjugated fluorophores to detect various targets within an immunofluorescence assay. In brief, samples were fixed at 4% Paraformaldehyde and embedded in paraffin. Serially cut sections of 5 μm were stained with haematoxylin and eosin for routine light microscopy, and used for immunohistochemistry. Depending on the antibody, antigen retrieval was performed in Citrate buffer at pH 6. Deparaffinized sections were then incubated overnight with primary antibodies against AQP1 (cat No. #AB2219, Millipore), NGFR (cat No. 8238, Cell Signalling Technology) and phospho-ERK1/2 Thr202/Tyr204 (Cat No. #4370, Cell Signalling Technology). Subsequently, the slides were washed in phosphate-buffered saline, pH 7.2, and incubated for 10 min at room temperature with Opal Polymer HRP Mouse Plus Rabbit secondaries (PerkinElmer). After another wash in PBS, the slides were then incubated at RT for 10 min with one of the following Alexa Fluorescent tyramides (PerkinElmer) included in the Opal 4 colour kit (NEL810001KT) to detect antibody staining, prepared according to the manufacturer's instructions: Opal 520, Opal 570 and Opal 690 (dilution 1:50).

Stripping of primary and secondary antibodies was performed by placing the slides in a plastic container filled with antigen retrieval (AR) buffer in Citrate pH 6; microwave technology was used to bring the liquid at 100 °C (2 min), and the sections were then microwaved for an additional 15 min at 75 °C. Slides were allowed to cool in the AR buffer for 15 min at room temperature and were then rinsed with deionized water and 1 × Tris-buffered saline with Tween 20. After three additional washes in deionized water, the slides were counterstained with DAPI for 5 min and mounted with ProLong™ Gold Antifade Mountant (Thermofisher Scientific). Slides were scanned for image acquisition using Zeiss AxioScan Z.1 and ZEN2 software.

### Multiplexed, sequential immunohistochemistry and analysis

Sequential chromogenic immunohistochemistry (IHC) was performed as previously described (Tsujikawa et al., 2017). In brief, 5 μm FFPE tissue sections of PDX samples were de-paraffinized, bleached (10% hydrogen peroxide at 65°C, 10 min), and subsequently stained with hematoxylin (GHS116, Sigma-Aldrich). Iterative cycles of standard IHC (heated antigen retrieval, Citra Plus, pH 6.2, BioGenex) were performed followed by detection with ImmPressTM IgG-polymerized peroxidase reagents (Vector Laboratories) and visualization with AEC (Vector Laboratories). Slides were scanned and subsequently, AEC was removed using ethanol and antibody stripped in heated citrate buffer to allow the next staining cycle. Complete antibody removal was confirmed at each step. Images were acquired using Aperio ImageScope AT (Leica Biosystems). Serial digitized images were processed using a computational image analysis workflow described previously (Tsujikawa et al., 2017) and images aligned and pseudo-coloured for visualization (Aperio ImageScope, Leica). Single-cell segmentation and quantification of staining intensity was performed using a CellProfiler v.2.1.1 pipeline. FCS Express 5 Image Cytometry v.5.01.0029 (De Novo Software) was used to gate intensity thresholds for subsequent analysis. Cell numbers extracted from FCS Express was used to generate image cytometry plots and plot relative proportions.

### FACS

Cells were incubated with GFRA2 (R&D systems, AF429) and NGFR (Cell Signalling Technology, #8238) antibody for 45 minutes at room temperature, followed by a secondary antibody conjugated with Alexa Fluor® 594 or Alexa Fluor® 647 for 30 min at room temperature. Cells were resuspended in FACS sorting buffer (culture medium supplied with 5% serum and 2 mM EDTA). FACS analyses were performed with BD FACSChorus™ and FlowJo® software.

### Single cell sorting and SMARTseq2 based scRNA sequencing

Single cell suspensions of MRD (DT/HX/PF) lesions were obtained as previously described (Rambow et al., 2018). DAPI negative, CD44-positive cells were sorted (BD Influx) in 96 well plates (VWR, DNase, RNase free) containing 2 μl of lysis buffer (0.2% Triton X-100, 4U of RNase inhibitor, Takara) per well. Plates were properly sealed and spun down at 2000 g for 1 min before storing at -80°C. SMART-seq2 based scRNaseq was performed as previously described (Rambow et al., 2018). NCSC signature activity (Rambow et al., 2018) per single cell was inferred using AUCell (Aibar et al., 2017).

### Targeted scDNA sequencing

Nuclei were extracted from a fresh frozen MEL015 treatment-naïve tumour sample according to the manufacturer's protocol (Tapestri, missionbio). Single-cell sequencing was performed using Mission Bio's Tapestri THP platform, which assesses hotspot mutations in about 50 genes, according to the manufacturer's protocol. Nuclei were emulsified with lysis reagent and incubated at 50°C prior to thermally inactivating the protease. The emulsion containing the lysates from protease-treated single-cells was then microfluidically combined with targeted gene-specific primers, PCR reagents, and hydrogel beads carrying cell identifying molecular barcodes using the Tapestri instrument and cartridge. Following generation of this second, PCR-ready emulsion, molecular barcodes were photocleavably released from the hydrogels with UV exposure and the emulsion was thermocycled to incorporate the barcode identifiers into amplified DNA from the targeted genomic loci. The emulsions were then broken using perfluoro-1-octanol and the aqueous fraction was diluted in water and collected for DNA purification with SPRI beads (Beckman Coulter). Sample indexes and Illumina adaptor sequences were then added via a 10 cycle PCR reaction and the amplified material was then SPRI purified a second time. Following the second PCR and SPRI purification, full-length amplicons were ready for quantification and sequencing. Libraries were analysed on a DNA 1000 assay chip with a Bioanalyzer (Agilent Technologies), and sequenced on the Illumina HiSeq2500 platform (PE150bp, rapid mode). Sequencing data were processed using Mission Bio's Tapestri Pipeline (trim adapters using cutadapt, sequence alignment to human reference genome hg19, barcode demultiplexing, cell-based genotypecallingusing-GATK/Haplotypecaller). Data were analysed using MissionBio's Tapestri Insights software package and visualized using R software.

### Droplet based scRNA sequencing

We profiled 4 PDX melanoma lesions (MEL006: 1xT0, 1xMRD and MEL015: 1xT0, 1xTres) using 3' scRNA sequencing (10x genomics) with a target cell recovery ranging from 5-10k cells per sample. Libraries for single cell RNA sequencing were constructed using the 10X Genomics Chromium platform according to manufacturer's instructions. Library construction was primarily done with the Chromium Single Cell 3' GEM, Library & Gel Bead Kit v3. In brief, cells were partitioned into Gel Bead-In-Emulsions (GEMs) at limiting dilution, where lysis and reverse transcription occurred yielding uniquely barcoded full-length cDNA from poly-adenylated mRNA. GEMs were subsequently broken and the pooled fraction was amplified, followed by fragmentation, end repair and adaptor ligation of size selected fractions. Transcriptome libraries were sequenced with paired end reads on an Illumina NovaSeq6000. After quality control, the raw sequencing reads were aligned to the human reference genome v. GRCh38 and mouse reference genome (mm10), followed by application of CellRanger (10x Genomics, v2.0) in order to obtain feature-barcode matrices. Cells with higher mapping results to the mouse genome were removed as well as potential doublets using the DoubletFinder v. 2.0.2 pipeline. Raw count matrices were analysed using R package Seurat v. 3.1.3. The matrices were filtered by removing cell barcodes with <1000 expressed genes, >9000 expressed genes and >30% (for T0 samples) and >50% (for MRD samples) of reads mapping to mitochondrial genes.

### Targeted bulk DNaseq

DNA extraction from fresh frozen minced PDX tumour tissue was performed using the DNeasy Blood & Tissue kit (Qiagen) according to the manufacturer's instructions. DNA was quantified using the Qubit 2.0 fluorometer (Life Technologies, Carlsbad, CA, USA). Next generation sequencing analysis for hotspot mutations was performed with the Illumina TruSight Tumor 26 kit (Illumina) or an in-house developed 96 cancer gene panel described elsewhere in more detail ([Vanden Bempt et al., 2021](#)). In addition, we performed a cluster analysis on the 96 cancer gene panel samples with a focus on the two models: MEL003 and MEL047. We aimed to identify commonly gained or lost mutations in each model, comparing the resistant lesions to the drug naïve lesion. Exonic mutations detected in the resistant lesions were kept regardless of their detection in the model-specific naïve lesion but were filtered out if they were present in more than one of the four other naïve lesions for low frequent variants (allele frequency smaller or equal 25%). The absolute difference between the mean allele frequency of resistant lesions versus the allele frequency of the naïve lesion was required to be bigger than 8%, the relative change bigger than 10%, the standard deviation smaller than 10%. A gnomad genome allele frequency smaller than 0.1 or undefined was required. The remaining list of variants was examined for their pathogenicity and their clinical relevance using a routine diagnostic workflow as described elsewhere ([Froyen et al., 2019](#)). In addition to the initial BRAF driver mutation no clinically relevant variants were retained.

### Copy number analysis

Genomic DNA was extracted for MEL006 and MEL015 T0 and Tres using the DNeasy Blood & Tissue kit (Qiagen) according to the manufacturer's instructions. DNA samples were quantified using UV absorbance, and SNPs at  $\pm$  300,000 sites were determined using the whole genome scanning 12-sample Illumina HumanCytoSNP-12v2.1 BeadChip according to the manufacturer's instructions. Images were captured on Cytoscan (Illumina), and data were primarily analysed using Illumina's GenomeStudio software.

Allele-specific copy number and sample purities were inferred using ASCAT (v2.5.2) after germline genotype prediction from the tumour BAF and correction of the LogR for GC-content biases ([Van Loo et al., 2010](#)).

### Whole-exome sequencing

Genomic DNA was extracted from MEL006 PDX tumour samples (T0 and Tres) using the DNeasy Blood & Tissue kit (Qiagen). Exome sequencing was performed at the Genomics Core Facility, KU Leuven, Leuven, Belgium. Exome capture was performed with the SeqCap EZ Human Exome Library v3.0 (NimbleGen). These samples were subsequently sequenced in a paired end 151 bp run on a Novaseq instrument (Illumina, San Diego, CA) resulting in an average coverage of 120x.

### Exome sequencing analysis

Reads were aligned separately to the human (hs38) and mouse (mm10) reference genome using BWA mem (0.7.15-r1140, bwakit). Bamcmp (5cb0176) was used to deconvolve human and mouse reads ([Khandelwal et al., 2017](#)). Confident somatic short variants (PASS SNVs and indels) were subsequently called on the human BAM files using GATK (v4.1.2.0) following the Somatic Short Mutation calling Best Practice Workflow. Mutect2 was run in tumour-only mode on T0 and considering T0 as matched control for Tres. Variants were annotated using Funcotator. Variant allele frequencies were converted to cancer cell fractions in R using the estimated tumour purity and local total copy number ([Dentro et al., 2017](#)) as inferred by ASCAT on the corresponding SNP array data. Exposures of mutational signatures previously identified in whole-genome sequenced melanoma samples (COSMIC v3) were estimated using sigfit (v1.3.2) running 100 Markov Chain Monte Carlo (MCMC) simulations for 10,000 iterations including a 5,000 iteration burn-in ([Gori and Baez-Ortega, 2018](#)).

### Stem and lineage score assessment

Stemness and melanoma-lineage identities were inferred from scRNAseq data for different drug tolerant cell states ([Rambow et al., 2018](#)). For this purpose, the transcriptional activity of a melanoma stemness related gene set, which is induced upon exposure of melanoma cells to hESC medium ([Peretz et al., 2015](#)), was quantified for each single cell using AUCell based scoring ([Aibar et al., 2017](#)) and served as a proxy for stemness. Similarly, a gene set for melanoma-lineage identity ([Rambow et al., 2015](#)) was quantified in each single cell. Finally, drug tolerant cells of the undifferentiated, NCSC and hyperdifferentiated state were injected into a two-dimensional stemness/lineage space based on corresponding AUCell scores.

### GDNF ELISA

Cells were cultured and treated on a 96well plate in a total volume of 200ul. 100ul supernatant was used to determine GDNF concentration by ELISA according to manufacturer's protocol (GDNF Emax® ImmunoAssay Systems, Promega). The plate with the remaining 100ul supernatant was used to determine cell numbers via Cell Titer Glo Assay according to manufacturer's protocol (Promega).

### Sanger sequencing

Tumours were lysed and gDNA extracted with the NucleoSpin DNA RapidLyse kit according to manufacturer's protocol (Machery-Nagel). NRAS exon3 was amplified out of 100ng gDNA via PCR and sent for Sanger sequencing. PCR protocol and primer sequences are available upon request.

### BRAF-splicing PCR

Between 200-300ng total RNA was used as input in a 20 $\mu$ l (total volume) SuperScript III (Invitrogen) RT reaction using oligo dT primers. We used 5 $\mu$ l of this cDNA reaction as input for the following PCR (50 $\mu$ l total volume): 5 $\mu$ l of Phusion High-Fidelity 10xPCR buffer (ThermoFisher), 1.5 $\mu$ l 10mM dNTP, 1.5 $\mu$ l 10  $\mu$ M Fwd primer (*BRAF* trunc F-5'-GGCTCTGGTTATAAGATGGC-3'), 1.5 $\mu$ l 10  $\mu$ M Rev primer (*BRAF* trunc R-5'- ACAGGAAACGCACCATATCC-3'), 1 $\mu$ l 50mM MgSO<sub>4</sub>, 0.5 $\mu$ l Phusion High-Fidelity Taq polymerase and up to 45 $\mu$ l with water. Thermocycling conditions: 94°C 5min 1 cycle, 94°C 15sec\_55°C 30sec\_68°C 3min 38-40cycles, 68°C 5min 1cycle. Gel purify PCR-bands and Sanger-sequence with PCR primers ([Pupo et al., 2017](#)). The amplicon corresponding to *BRAF* WT is 2301bp. The alternative splicing variants are detected with amplicons of 1665bp for Δexon 4-8 and 1299bp for Δexon 2-8.

### Meta-analysis of resistance mechanisms to MAPK inhibition

DNA sequencing of BRAFi&MEKi resistant *BRAF*-mutant melanoma patients of three centers was reassessed for the presence (genetic) or absence (non-genetic) of genetic alterations at resistance ([Hugo et al., 2015](#); [Kwong et al., 2015](#); [Long et al., 2014](#); [Rizos et al., 2014](#)). The percentage of genetic and non-genetic events was stratified by either number of samples or patients ([Table S1](#), DNA summary).

### Meta-analysis of NCSC signature induction upon MAPK inhibition

Bulk-RNA sequencing data of matched treatment naïve and ON-treatment (BRAFi&MEKi) melanoma samples of three centers ([Hugo et al., 2015](#); [Kwong et al., 2015](#); [Long et al., 2014](#); [Rizos et al., 2014](#)) were interrogated for an induction of the NCSC gene expression program. Briefly, gene count matrices were rendered non-zero and subsetted for the NCSC gene signature (n=42). Ratios for each gene were determined by comparing matched treated vs. baseline sample generating a gene (ratio) x sample matrix (42x49samples), which was objected to PCA. Furthermore, the average of all 42 ratios per sample was calculated and used to infer NCSC-enrichment. When projecting the sample-pairs into the PCA1 and PCA3 space, NCSC\_enriched samples dispersed from the center. These corresponded conclusively to the NCSC\_enriched samples with an average ratio>1.73 ([Figure 1C](#)), hence ratio>1.73 was set as enrichment cut-off ([Table S1](#), RNA summary).

### Data availability

Targeted DNA sequencing data (TruSight, Illumina) of the different PDX models were submitted to the European Genome Archive (EGAS00001005314) as well as whole-exome sequencing and SNP array data of MEL006 and scRNAseq of MEL006 and MEL015.

**QUANTIFICATION AND STATISTICAL ANALYSIS**

Unpaired Student t-test, Mann-Whitney U and log Rank progression free survival analysis were performed using GraphPad Prism version 9.00 for Mac, GraphPad Software, La Jolla California USA, [tumor.graphpad.com](http://tumor.graphpad.com).